Palaeogeography, Palaeoclimatology, Palaeoecology 631 (2023) 111831

Contents lists available at ScienceDirect

Palaeogeography, Palaeoclimatology, Palaeoecology

journal homepage: www.elsevier.com/locate/palaeo

Deciphering the termination of the Messinian salinity crisis: The alkenone record of the Miocene-Pliocene transition in the northern Mediterranean.

F. Pilade [a,*], I. Vasiliev [b], D. Birgel [c], F. Dela Pierre [a], M. Natalicchio [a], A. Mancini [a], G. Carnevale [a], R. Gennari [a]

[a] Dipartimento di Scienze della Terra, Università di Torino, Via Valperga Caluso 35, 10125 Torino, Italy
[b] Senckenberg Biodiversity and Climate Research Centre, Senckenberganlage 25, 60325 Frankfurt am Main, Germany
[c] Institut für Geologie, Centrum für Erdsystemforschung und Nachhaltigkeit, Universität Hamburg, Bundesstraße 55, D-20146 Hamburg, Germany

ARTICLE INFO

Editor: M. Zhao

Keywords:
Molecular fossils
Stable isotopes
Messinian salinity crisis
Sea surface temperature
Sea surface salinity

ABSTRACT

The late Miocene Messinian salinity crisis (MSC; 5.97–5.33 Ma) transformed the Mediterranean basin into the youngest salt giant in Earth history. The paleoenvironment and the paleodepth of the Mediterranean basin during the terminal phase of the MSC (i.e., the Lago-Mare event), are still uncertain, primarily due to the contradicting presence of in-situ, fully marine vs brackish to freshwater fossils, with different palaeoecological affinity, found in the same rock record. This study uses the distribution of C_{37}, C_{38} and C_{39} long-chain unsaturated methyl and ethyl n-ketones (alkenones), produced by haptophyte algae, in combination with micropaleontological and stable oxygen isotope data, to reconstruct the surface water temperatures and paleoenvironmental conditions in the Northern Mediterranean basin across the transition between the latest Miocene Lago-Mare phase to the re-establishment of marine conditions starting in Pliocene, at 5.33 Ma. The results suggest that the Mediterranean basin was already receiving influxes from the Atlantic Ocean before the end of the MSC, resulting in a progressive return to marine conditions proceeding from south to north, i.e., from the more distal to proximal areas. Finally, fully marine conditions were established at the base of the Pliocene (5.33 Ma). The study highlights the reliability of alkenone-based paleo proxies for environmental reconstruction, especially when body fossil records of primary producers are scarce or problematic.

1. Introduction

During the Messinian salinity crisis (MSC) of the late Miocene (5.97-5.33 Ma), the Mediterranean basin was transformed into the youngest salt giant in Earth history, following its partial isolation from the Atlantic Ocean caused by the tectonic restriction of the (paleo) Gibraltar gateways (Hsü et al., 1973; Cita, 1982; Rouchy and Caruso, 2006; Ryan, 2011; Roveri et al., 2014a; Krijgsman et al., 1999; Capella et al., 2020). The sedimentary record of the MSC consists of more than 1 million km^3 of evaporites (gypsum, anhydrite, halite), deposited in less than 640 kyr following an alleged high magnitude (600–1500 m) sea level drawdown (see Roveri et al., 2014b; Gvirtzman et al., 2022).

After the acme, the terminal phase of the MSC is characterized by peculiar brackish sediments that define the so-called Lago-Mare event (5.53-5.33 Ma; CIESM, 2008; Andreetto et al., 2021 and references therein). The Lago-Mare sediments are abruptly overlain by Zanclean open marine deposits that end the MSC at 5.33 Ma (Rouchy and Caruso, 2006). The nature of the return to the marine conditions is still under discussion. Generally, there is an agreement that marine conditions were restored from the base of the Pliocene (Zanclean), which is characterized by sediments with well-preserved marine calcareous microfossil assemblages (Di Stefano et al., 1996; Iaccarino et al., 1999; Gennari et al., 2008; Di Stefano and Sturiale, 2010; Corbí et al., 2016; Caruso et al., 2020). Calcareous microfossils suggest bathyal paleodepths (Iaccarino et al., 1999), although shallow water environments were documented in marginal basins of the northern Apennines (Artoni et al., 2004; Gennari et al., 2008) and Spain (Roveri et al., 2020). However, the paleoenvironment and paleodepth interpretations of the latest Messinian Lago-Mare event have not been solved yet (e.g., Andreetto et al., 2022b). There is still a debate resulting in radically different interpretations of the demise of the MSC. One of the proposed hypotheses suggests that during the Lago-Mare event, the Mediterranean consisted of numerous disconnected endorheic lakes fed by local rivers (Rouchy and Caruso, 2006; Amadori et al., 2018; Orszag-Sperber, 2006; Caruso et al., 2020),

* Corresponding author.
E-mail address: francesco.plilade@unito.it (F. Pilade).

https://doi.org/10.1016/j.palaeo.2023.111831
Received 10 July 2023; Received in revised form 19 September 2023; Accepted 28 September 2023
Available online 2 October 2023

which were abruptly filled by catastrophic flooding of Atlantic water, induced by the collapse of the Gibraltar sill (Hsü et al., 1973; Garcia--Castellanos et al., 2020; Amarathunga et al., 2022). Such a scenario seems to be supported by the observation of flooding-related erosional features in seismic profiles from the western Mediterranean (Garcia--Castellanos et al., 2009), by chaotic flood deposits of alleged Zanclean age in the western Ionian Sea (Micallef et al., 2018; Garcia-Castellanos et al., 2020) and by contourites (Arenazzolo Fm.) just under the Messinian-Zanclean boundary exposed on land in Sicily (Van Dijk et al., 2023). Alternatively, the Mediterranean was already connected with the Atlantic Ocean during the latest Messinian and was gradually refilled (Marzocchi et al., 2016; Merzeraud et al., 2019). The latter interpretation was proposed independently based on the brackish (Roveri et al., 2014a; Andreetto et al., 2021; Bulian et al., 2022) or marine environments established before the Zanclean (Aguirre and Sánchez-Almazo, 2004, Carnevale et al., 2006, Schwarzans and Carnevale, 2022). These different interpretations (catastrophic flooding vs gradual refilling and brackish vs marine Lago-Mare environment) are fuelled by the ambiguity of the origin of body fossil record of the Lago-Mare sediments, which is either composed of freshwater to brackish euryhaline ostracods and mollusks (Bonaduce and Sgarrella, 1999; Iaccarino et al., 1999; Taviani et al., 2007; Esu and Girotti, 2008; Gliozzi and Grossi, 2008) or also marine biota represented by remains of marine fishes and calcareous microfossils (Aguirre and Sánchez-Almazo, 2004; Carnevale et al., 2006, 2008, 2018, 2019; Popescu et al., 2008, Clauzon et al., 2015, Andreetto et al., 2022a). Alternatively, these marine and brackish fossils are considered reworked from older sediments (Andreetto et al., 2021) or displaced by more marginal settings (Aguirre and Sánchez-Almazo, 2004), respectively.

In this contribution, we combined organic (long-chain alkenones based proxies) and inorganic (oxygen stable isotopes on foraminifera and ostracods) geochemical data together with the micropaleontological assemblages (foraminifera, calcareous nannofossils, ostracods), to reconstruct the environmental changes at the end of the Lago-Mare phase and across the Messinian-Zanclean boundary.

Long-chain alkenones (LCA) are unsaturated long-chain methyl and ethyl n-ketones produced by coccolithophorids, haptophyte algae (Henderiks et al., 2022) living in the upper photic zone. The degree of unsaturation of LCA depends on the temperature of waters harbouring their source organisms, a direct relationship that can be traced through the U^{k}_{37} index, which linearly increase with higher temperature and decrease with lower temperatures (Brassell et al., 1986; Conte et al., 1998; Marlowe et al., 1984; Müller et al., 1998; Herbert et al., 2016). The U^{k}_{37} was calibrated with modern sea surface temperatures (SST) (Conte et al., 2001; Conte et al., 2006; Müller et al., 1998; Prahl and Wakeman, 1987; Prahl et al., 1988) and consequently allowed the reconstruction of paleo SST fluctuations in Quaternary sediments (i.e., Gould et al., 2017; Rice et al., 2022). LCA-based SSTs were also applied to the Late Miocene (Tzanova et al., 2015; Herbert et al., 2016), but no data existed for the MSC, although LCA were found in the late Messinian Upper Gypsum sediments of the Eraclea Minoa section in Sicily (Southern Italy) (Vasiliev et al., 2017).

The recovery of LCA in modern and ancient brackish and freshwater environments has revealed that LCA producers are not confined solely to marine environments (Chu et al., 2005; Wang et al., 2015; Huang et al., 2021). Within this context, identifying the specific type of LCA (marine, freshwater, brackish water, or a mixture) within ancient sediments holds great promise for reconstructing paleoenvironments. This is particularly true because, although we cannot entirely exclude the possibility of reworking, it is noteworthy that reworking of LCA is generally considered as an unlikely process (e.g., Kucera, 2019).

We provide an alkenone-based paleo SST record for the latest Messinian-Early Zanclean interval that implements the available datasets (Herbert et al., 2016; Vasiliev et al., 2017; Tzanova et al., 2015) to better understand the history of the Mediterranean basin in this critical time interval. For the same interval and for the first time, SST data are combined with stable isotope geochemical analyses on calcareous microfossils to quantitatively constrain the Mediterranean Sea surface salinity (SSS). Finally, we aimed to reconstruct the environmental changes across the Messinian-Zanclean boundary proposing a possible mode of the termination of the MSC in the northern Mediterranean basin, using three sections located along a SE-NW transect in the Northern Apennine chain, from deeper water in the south to coastal areas in the north.

2. Geological setting

The N to NE verging Northern Apennine fold and thrust belt (Fig. 1A) developed since the Cenozoic in response to the convergence between the European and African plates (Carminati and Doglioni, 2012). Following the Oligocene-Miocene continental collision, deposition occurred within NW-SE elongated foredeep basins, which developed at the front of the belt. At the top of already accreted internal units (e.g., Cretaceous to Eocene Ligurian units) smaller wedge-top basins were established (Ricci Lucchi, 1986).

From SE to NW three sectors can be distinguished (Artoni et al., 2007): a) the Marche and Romagna sector (MR; Fig. 1A, C), corresponding to the Middle to Late Miocene foredeep; b) the central Emilia sector (cE; Fig. 1A, C), characterized by small Eocene to Messinian wedge-top basins (Epiligurian basins) developed at the top of deformed Ligurian units; and c) the Piedmont Basin (PB; Fig. 1A, C), where Eocene to Messinian sediments are floored by Alpine, Ligurian and Adriatic basement units (Mosca et al., 2010).

The uppermost Messinian succession is composed of post-evaporitic terrigenous sediments deposited between 5.53 and 5.33 Ma (Fig. 1C; MSC stage 3; CIESM, 2008). These deposits are floored by clastic evaporites grouped into the Resedimented Lower Gypsum unit (MSC Stage 2, 5.60-5.53 Ma). They were sourced by the erosion of primary gypsum deposits of MSC Stage 1 (5.97-5.60 Ma) that were uplifted and eroded following an intra-Messinian tectonic phase (ca. 5.60 Ma; Manzi et al., 2007; Roveri et al., 2014a).

In the Marche and Romagna and central Emilia sectors the post-evaporitic (p-ev) sediments are subdivided into two units (Fig. 1B) (Artoni et al., 2004; Roveri et al., 2008b): a) the p-ev1 unit, consisting of fine-grained sediments with a coarsening upward trend (Roveri et al., 1998); b) the p-ev2 unit (Fig. 1B), consisting of alternations of coarse and fine-grained sediments of fluvial-deltaic, prodeltaic and basinal environments (Iaccarino and Papani, 1979; Roveri et al., 2008b). In the Marche and Romagna sector, a U—Pb dated ash layer (5.532 ± 0.0046 Ma) is present in the p-ev1 unit of the Maccarone section (Cosentino et al., 2013; Fig. 1B). Four lithological cycles with coarse and fine-grained sediments were recognized in the p-ev2 unit. These cycles were tuned to the insolation curve, allowing dating the succession between 5.42 and 5.33 Ma (Roveri et al., 2008b). The base of the p-ev2 unit marks a drastic change in the sedimentation, reflecting a transgressive trend on the basin margins from 5.42 Ma (Roveri et al., 2008b). In the Marche and Romagna sector, the uppermost three cycles contain three fine-grained carbonate beds termed 'Colombaccio' (col1, 2 and 3; Bassetti et al., 2004; Fig. 1B), correlating to insolation maxima (Roveri et al., 2008b). A similar succession was found in the central Emilia sector (Artoni et al., 2007).

In the Piedmont Basin, the post-evaporitic sediments are represented by the Cassano Spinola Conglomerates. In the lower part, this unit consists of fluvial deposits with remains of terrestrial fossils (Colombero et al., 2013; Carnevale et al., 2018), grading upwards to clays and marls with Lago-Mare ostracods and mollusks, mixed with marine calcareous nannofossils and dinocysts (Andreetto et al., 2022a).

As for the rest of the Mediterranean, the mixing of freshwater, brackish and marine microfossils have generated an intense debate on the nature of the Lago-Mare phase and of p-ev units of the Northern Apennine, which is still unsolved (Andreetto et al., 2021). According to some authors (Roveri et al., 2008c; Grossi et al., 2008; Stoica et al.,

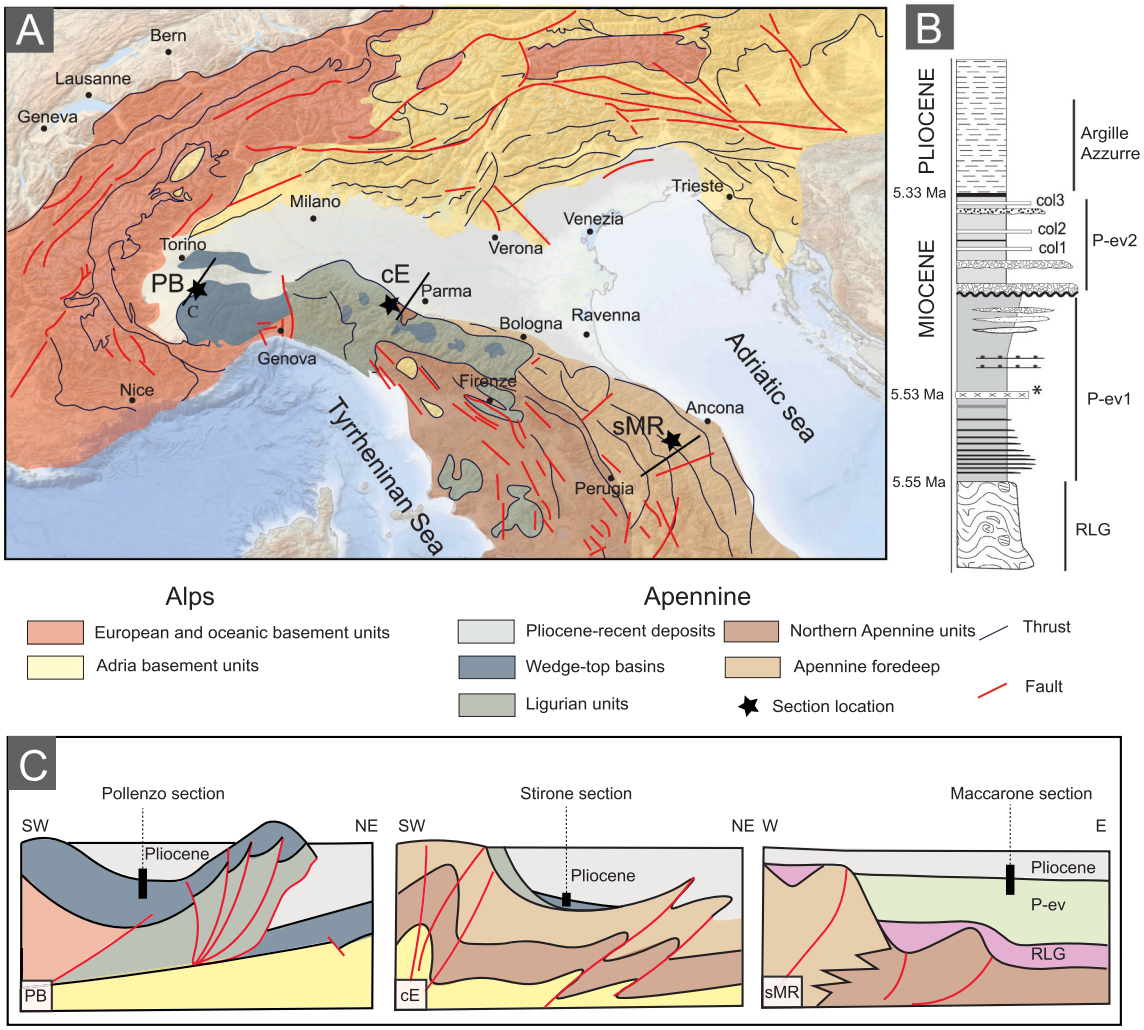

Fig. 1. A) Simplified geological map of the Northern Apennine (adapted from Bigi et al., 1989, Artoni et al., 2007; Roveri et al., 2008b). The three studied sectors are indicated: PB) Piedmont Basin; cE) Central Emilia sector; sMR) Marche and Romania sector); the bold lines indicate the cross section as shown in B. B) Schematic cross section of the upper Messinian – lower Zanclean succession of the Northern Apennine (adapted from Roveri et al., 2008b). C) Simplified cross sections of the three study areas showing the geodynamic context (adapted from Artoni et al., 2007; Mosca et al., 2010; Roveri et al., 2008b). RLG: Resedimented Lower Gypsum unit; p-ev1 and p-ev2: post-evaporitic 1 and 2, respectively; col1, col2, col3: Colombaccio layers (Bassetti et al., 2004); the asterisk marks the ash layer (Cosentino et al., 2013) intercalated in the p-ev1 unit.

2018; Grothe et al., 2018) fluvio -deltaic sediments and fresh to brackish water body fossils of the p-ev units indicate that the marine microfossils (calcareous plankton and otoliths of marine fish) (Popescu et al., 2008; Carnevale et al., 2018) are reworked. Accordingly, Pellen et al. (2017), considered the Northern Apennine foredeep from 5.60 to 5.33 Ma as a large perched and isolated brackish-to-freshwater basin disconnected from the central Mediterranean by an emerged sill (the Gargano-Pelagosa sill), located to the south of the investigated area (see also Amadori et al., 2018, and Andreetto et al., 2022b.)

The end of the MSC in the northern Mediterranean is marked by the deposition of open marine marls and clays (Argille Azzurre Fm.), starting at 5.33 Ma (Gennari et al., 2008; Trenkwalder et al., 2008; Violanti et al., 2011) as in other Mediterranean sections (Iaccarino et al., 1999). The Messinian-Zanclean boundary (MZB) is commonly marked by a characteristic dm-thick dark layer (Iaccarino and Papani, 1979; Gennari et al., 2008; Violanti et al., 2011). Similar dark layers were also described in the western (Iaccarino et al., 1999; Bulian et al., 2022) and eastern sectors (Amarathunga et al., 2022) of the Mediterranean.

3. Material and methods

3.1. Studied sections

We studied three sections (Fig. 1); from SE to NW, they are:1) Maccarone (Marche-Romagna sector), 2) Stirone (central Emilia sector) and 3) Pollenzo (Piedmont Basin).

3.1.1. Maccarone section

The Maccarone section (Odin et al., 1995; Bertini and Martinetto, 2011) is in the Northern Apennine main foredeep (43°24′02.3" N 13°06′26.2" E; Fig. 2A) and comprises p-ev1 (with the 5.532 ± 0.0046 Ma ash layer; Cosentino et al., 2013), p-ev2 and Zanclean deposits. The studied interval is 13.95 m-thick and consists of the uppermost p-ev2 (Lago-Mare) and lowermost Zanclean deposits (Fig. 3); the basal Colombaccio layer (col2 of Bassetti et al., 2004) and the overlaying 30 cm-thick dark layer (DL1) were not sampled. Above the DL1, 8.10 m of grey silty marls alternating with cm-thick siltstones and sandstones occur, followed by a second 50 cm-thick Colombaccio layer (col3 of Bassetti et al., 2004), which is overlain by 40 cm of dark grey laminated marls (DL2). The upper part of the Messinian p-ev2 unit consists of one

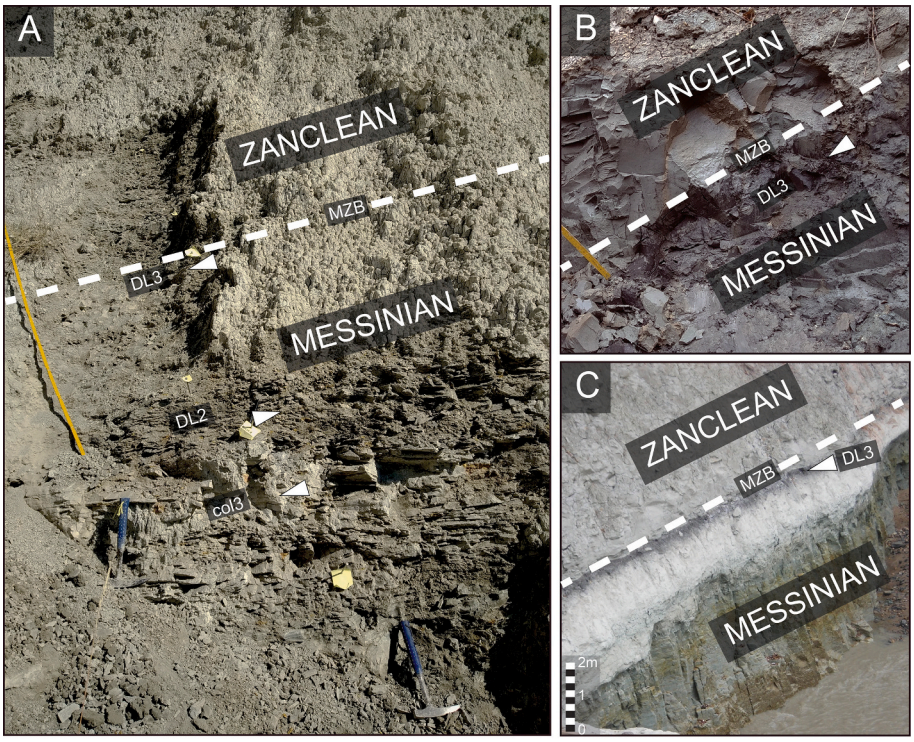

Fig. 2. The Messinian – Zanclean transition in: A) Maccarone; B) Stirone and C) Pollenzo sections. col3: uppermost Colombaccio layer in the Maccarone section (see Bassetti et al., 2004); DL2: dark layer above the col3; DL3: dark layer at the Messinian - Zanclean boundary. White arrows indicate the mentioned layers.

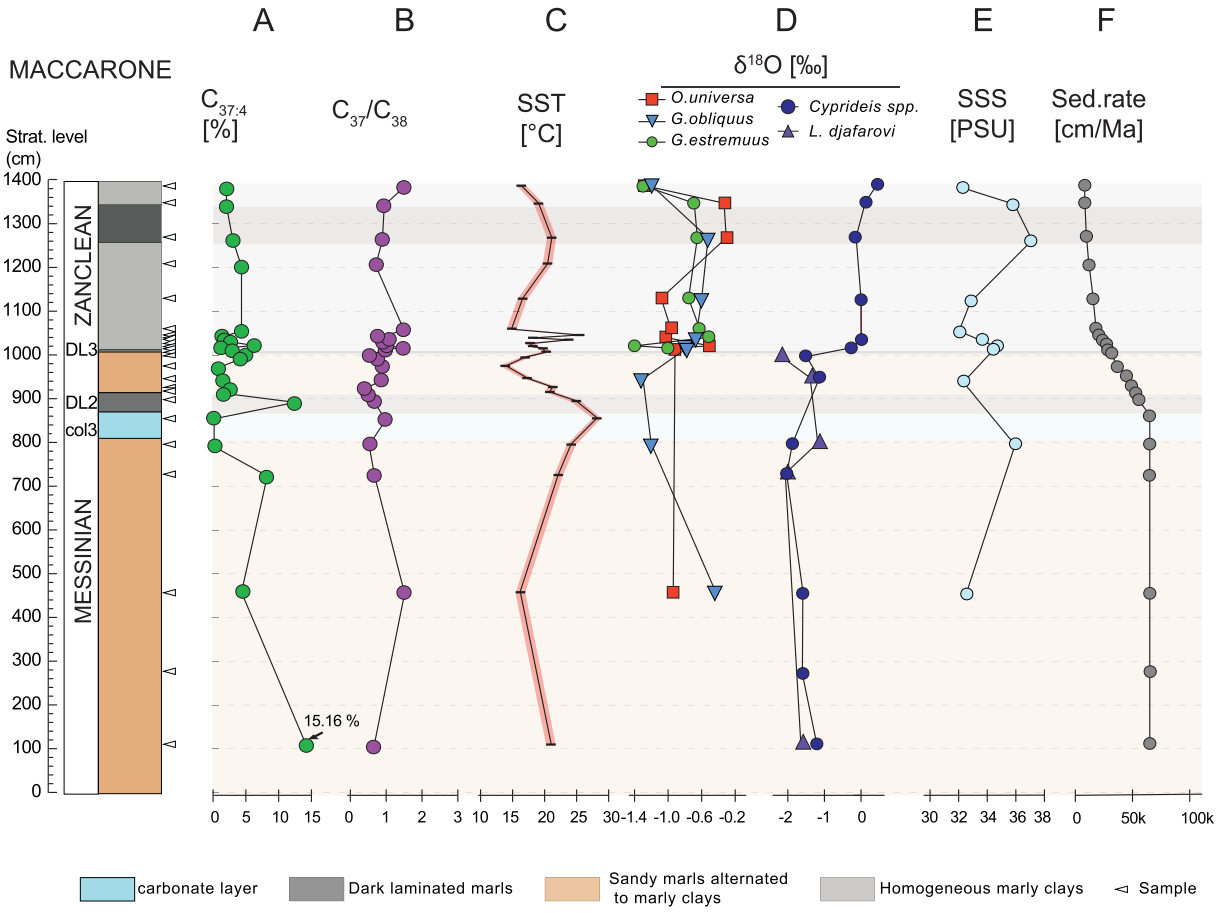

Fig. 3. Schematic lithological log with sampled levels (white arrowheads) and results for the Maccarone section. A) C37:4[%]; B) C_{37}/C_{38} ratio; C) Sea surface temperature (SST); black bars indicate the error range; D) $\delta^{18}O$ values of planktonic foraminifera and ostracods; E) sea surface salinities (SSS); F) sedimentation rate.

meter of light grey homogeneous marls with thin sandstone intercalations. The MZB is marked by a 10 cm thick layer of black bioturbated sandstones (DL3). The Zanclean deposits belonging to the Argille Azzurre Fm. are represented by 2.8 m of clays, intercalated by 80 cm of laminated dark grey marls. These sediments were dated using bio-, cyclo- and magnetostratigraphy by Gennari et al. (2008).

3.1.2. Stirone section

In the Stirone section (44°50′12.1"N 9°57′58.5"E; Iaccarino and Papani, 1979), the uppermost Messinian (Lago-Mare) to Lower Pliocene succession is exposed; these deposits belong to a wedge top basin of the central Emilia sector of the Northern Apennine (Fig. 1A). After several meters of conglomerate and cross-bedded sandstone of fluvio-deltaic origin (Iaccarino and Papani, 1979), the sampled section starts with 13.35 m of silty marls with sandstone intercalations. In the lower part, the silty marls also include a 20 cm-thick interval consisting of thin micritic limestone layers, probably equivalent to the Colombaccio beds of the Marche and Romagna sector (Gennari et al., 2008; Artoni et al., 2007). In this section, the MZB is marked by a densely bioturbated 60 cm-thick dark clay-to-silt layer (DL3, Fig. 2B), which is overlain by 2 m of bioturbated marly clays belonging to the Zanclean Argille Azzurre Fm (Fig. 4).

3.1.3. Pollenzo section

The Pollenzo section (44°41′09.6" N 7°54′50.4" E) in the Piedmont Basin, comprises the entire MSC succession and the transition to the Zanclean (Dela Pierre et al., 2011; Andreetto et al., 2022a). The studied section refers to the uppermost 8.6 m of the succession (Fig. 2C). The lowermost 3.2 m consists of an alternation of brown silty marls and yellow sands representing the uppermost post-evaporitic unit, locally named Cassano Spinola Conglomerates. A dark 50 cm-thick clay layer (DL3), intensively bioturbated, marks the transition to the 4.9 m thick Zanclean claystones of the Argille Azzurre Fm. (Fig. 5).

3.2. Lipid Biomarker extraction, separation, and analytical approach

For lipid biomarker analysis, fifty sediment samples were collected from the three sections: Pollenzo (10 samples), Stirone (15 samples), and Maccarone (25 samples). To avoid potential contamination during sampling and the up-work procedure, the outermost part of each sample was discarded before sub-sampling for lipid extraction. The sediment samples (40-60 g each) were air-dried and ground to a homogeneous powder. Then, the powders were extracted at Senckenberg Biodiversity and Climate Research Centre (SBiK-F) in Frankfurt using a Soxhlet apparatus with a Dichloromethane (DCM) – Methanol (MeOH) (7.5:1; *v:v*) organic solvent mixture. The resulting total lipid extracts (TLE) were dried under continuous N_2 flow using a TurboVap LV. Elemental sulfur was removed from the TLEs using Cu shreds activated with 10% HCl and subsequently rinsed with MeOH, DCM and MilliQ water until neutral. The vials containing TLE, activated Cu and magnetic rods were placed on a rotary table for ~20 h. Afterwards, TLEs were filtered over a Na_2SO_4 column to remove particles, including Cu and Cu sulphides and any remaining potential water. An aliquot of the desulfurized TLE was separated at the University of Hamburg using a solid-phase silica gel column in a Pasteur pipette. The pipette was plugged with organic-solvent cleaned cotton, then filled with partially deactivated silica gel (4-5 cm). The silica gel column was cleaned with one column volume of DCM and then conditioned with 5 column volumes of n-hexane. 10% of the TLE was dissolved in 500 µl *n*-hexane and pipetted onto the column. The hydrocarbons were collected by using *n*-hexane as solvent. The ketones (including esters) were eluted with *n*-hexane/DCM (3:1). Then the alcohols were eluted by using a mixture of DCM/acetone (9:1).

For this study, only the ketone fraction was used. Aliquots of the ketone fraction were measured on the Gas Chromatograph coupled to Flame Ionization Detection (GC-FID) for LCA relative abundance integration and Gas Chromatography-Mass Spectrometry (GC–MS) for identification at the University of Hamburg. The identification of compounds was achieved by comparing retention times and published mass

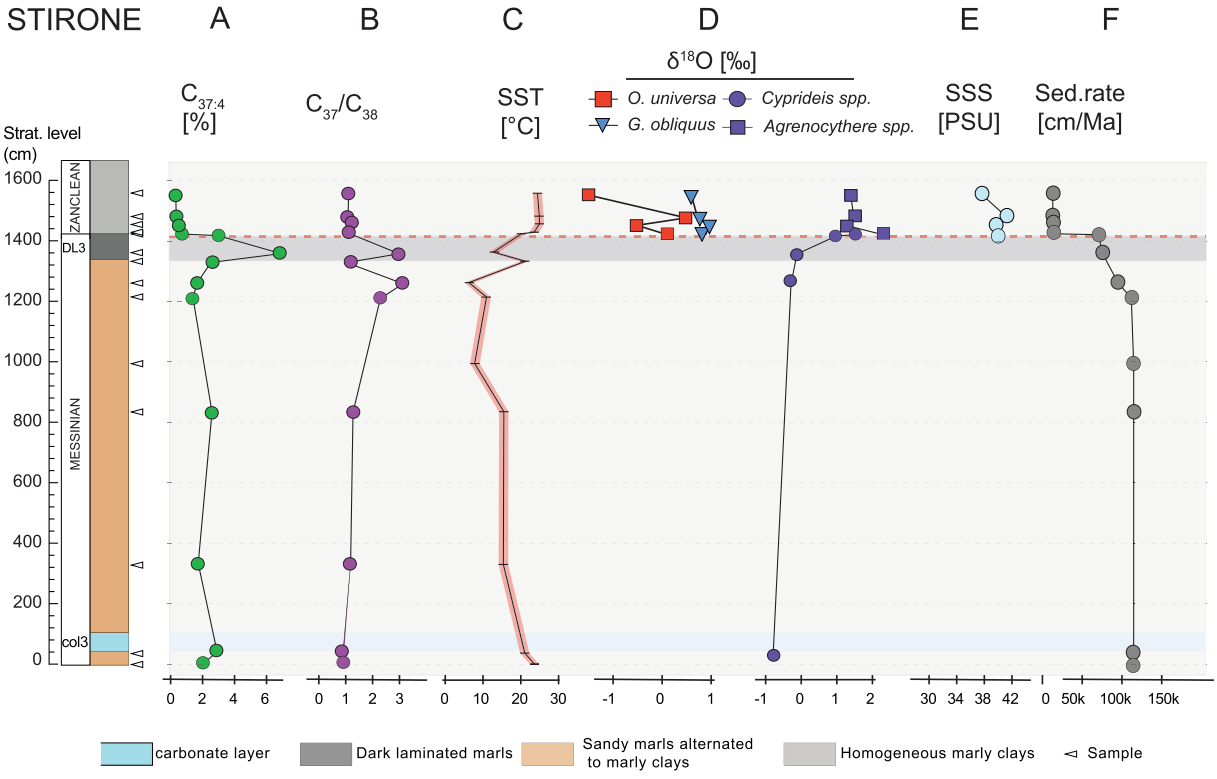

Fig. 4. Schematic lithological log with sampled levels (white arrowheads) and results for the Stirone section. A) C37:4[%]; B) C_{37}/C_{38} ratio; C) Sea surface temperature (SST); black bars indicate the error range; D) $\delta^{18}O$ values of planktonic foraminifera and ostracods; E) sea surface salinities (SSS); F) sedimentation rate.

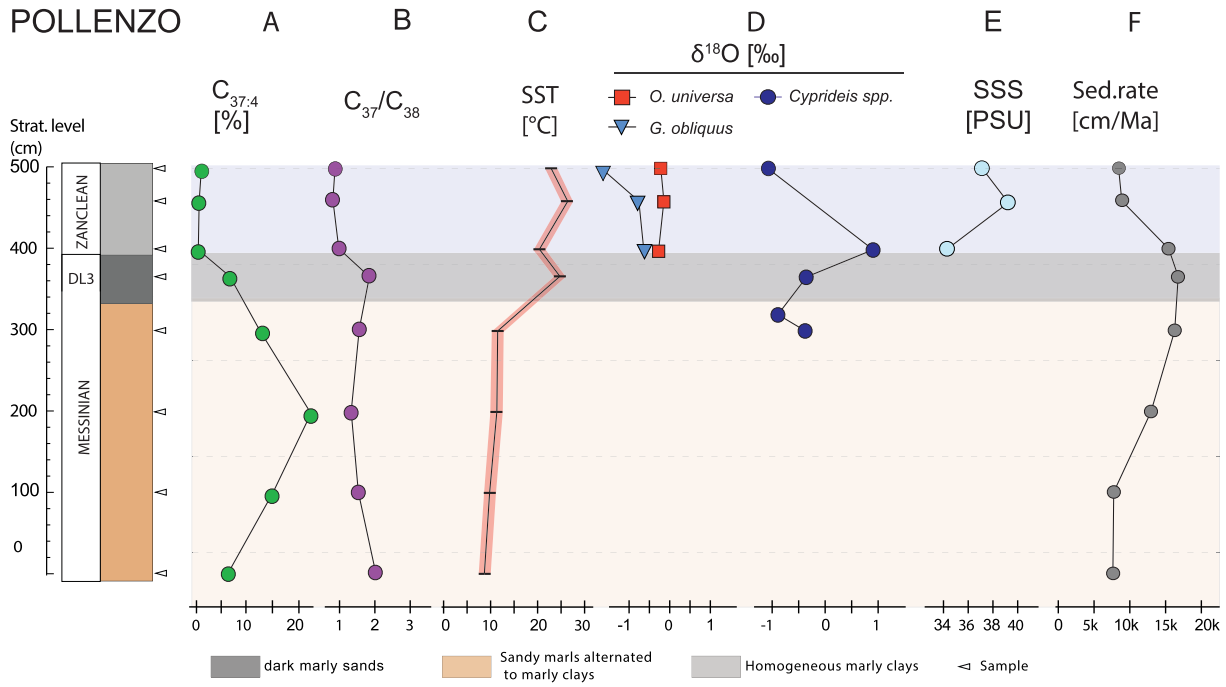

Fig. 5. Schematic lithological log with sampled levels (white arrowheads) and results for the Pollenzo section. A) $C_{37:4}$[%]; B) C_{37}/C_{38} ratio; C) Sea surface temperature (SST); black bars indicate the error range; D) $\delta^{18}O$ values of planktonic foraminifera and ostracods; E) sea surface salinities (SSS); F) sedimentation rate.

spectra using Xcalibur® software. No internal standards were added to the ketone fraction; therefore, we manually integrated the selected peaks in GC-FID chromatograms (chromatogram examples Fig. S4) with the Chromeleon ® software. Carrier gases used for the GC–MS and GC-FID analyses were helium and hydrogen, respectively. Both instruments were equipped with a *Thermo Fisher TG-5MS* fused silica column (30 m in length, 0.25 mm diameter, thickness film of 0.25 μm). The temperature program used for the GC was as follows: an initial temperature of 50 °C was maintained for 3 min, followed by a linear increase to 230 °C at a rate of 25 °C per minute, with a 2-min hold at 230 °C. Finally, the temperature was raised from 230 °C to 320 °C at a rate of 6 °C per minute and maintained at 320 °C for 20 min.

3.3. Analysis of long chain alkenones and sea surface temperature calculations

The long chain alkenone-based unsaturation index (U^{k}_{37}) is directly proportional to surface water temperature in various aquatic environments ranging from marine to continental (Prahl and Wakeman, 1987), and is based on the equation:

$$U^{k}_{37} = [C_{37:2} - C_{37:4}]/[C_{37:2} + C_{37:3} + C_{37:4}] \quad (1)$$

Eq. (1) was the first calibration used, but was not applied for Quaternary marine environments, because of the only minor amounts of $C_{37:4}$; due to this fact the $U^{k'}_{37}$ index is usually applied (Prahl and Wakeman, 1987; Müller et al., 1998; Conte et al., 2006; Herbert et al., 2016) which is defined as:

$$U^{k'}_{37} = [C_{37:2}]/[C_{37:2} + C_{37:3}] \quad (2)$$

The mean annual surface water temperature is based on a large and global dataset of open marine environments (Conte et al., 2006) and can be calculated according to the equation:

$$T = -(0.957) + 54.293 \times (U^{k'}_{37}) - 52.894 \times (U^{k'}_{37})2 + 28.321 \times (U^{k'}_{37}) \quad (3)$$

Eq. (3) has a residual standard (1σ) deviation of ±1.2 °C and was chosen for this study since it includes also numerous data points from the Mediterranean Sea. The $U^{k'}_{37}$ -based SST calibration, though, is derived from modern marine environments, where the dominant LCA producers are Coccolithophorids, especially *Emiliana huxleyi*, *Gephyrocapsa oceanica* and related species (Group III; Theroux et al., 2010, Wang et al., 2015). It has been shown that other groups of LCA producers (namely Group I and II) contribute significantly to the $U^{k'}_{37}$ at salinities lower than typical open marine values (between 31 and 39 PSU). If the signal of multiple LCA producers is preserved in sediments, the SST reconstructions are heavily biased due to the multi-species effect (Theroux et al., 2010). LCA originated by Group I (typical of freshwater) and II (typical of brackish water, from 0.5 to 30 PSU) and were recognized in lakes and brackish water bodies by DNA analyses and their respective LCA signature (Huang et al., 2021). If LCA originated by Groups I and II are present, alternative calibrations for SSTs in water with low salinities are used (Zink et al., 2001; Chu et al., 2005; Wang et al., 2021).

While the Pliocene sediments of this study were obviously deposited in a marine environment and therefore the SST calibration of Conte et al. (2006) can be confidently used, the Lago-Mare sediments are most likely variably attributed to marine, brackish, or freshwater environments or a mixture of the three (Pellen et al., 2017; Grossi and Gennari, 2008; Andreetto et al., 2021). Since DNA is not preserved in several million-year-old rocks, it is necessary to reliably evaluate the LCA composition during the Miocene-Pliocene transition and to verify the source groups of the LCA in our samples. Since LCA are referred to producers that thrive in different environments and using molecules unlikely reworked (Kucera, 2019), this evaluation is also helpful for paleoenvironmental reconstructions and will be used to disentangle the ambiguous body fossil record of the Lago-Mare sediments. This was done by using three indices introduced by Chu et al. (2005), Wang et al. (2015), Kaiser et al. (2019) and Huang et al. (2021): the $C_{37:4}$[%], the C_{37}/C_{38} ratio and the linear correlation between U^{k}_{37} and $U^{k'}_{37}$.

The $C_{37:4}$[%] is calculated as:

$$C_{37:4}[\%] = [C_{37:4}]/([C_{37:2}] + [C_{37:3}] + [C_{37:4}]) \times 100 \quad (4)$$

and its values are directly related to the group of LCA producers (Chu et al., 2005; Sun et al., 2007; Harada et al., 2008; Bendle et al., 2009;

Theroux et al., 2010; Theroux et al., 2013; Nakamura et al., 2014; D'Andrea et al., 2016; Longo et al., 2016; Huang et al., 2021).

The C_{37}/C_{38} ratio reflects the composition of LCA producer assemblages (Conte et al., 1998; Chu et al., 2005; Liu et al., 2011; Nakamura et al., 2014; Prahl et al., 1988; Wang et al., 2015; Zheng et al., 2019). It is calculated as the sum of all C_{37} divided by the sum of all C_{38} ($[\Sigma C_{37}]$ / $[\Sigma C_{38}]$).

Finally, the linear correlation between U^{k}_{37} and $U^{k'}_{37}$ was used by Wang et al. (2015) to unravel the multispecies effect. A high correlation between the two ratios indicates monospecific LCA contribution, while no significant correlation suggests a multi-species effect (Wang et al., 2015).

3.4. Micropaleontological analysis and SEM observations

Samples for micropaleontological analyses were disaggregated using a solution of H_2O: H_2O_2 (9:1; *v:v*). Subsequently, the samples were wet sieved to remove the <63 μm fraction and then dry sieved to obtain two size fractions (>125 μm, and 125–63 μm). Qualitative observations on the fraction >125 μm residues were performed and planktonic foraminifera and ostracod specimens were selected and hand-picked for subsequent stable isotope measurements. Smear slides were prepared according to the standard procedure outlined by Bown (1998) and used for semi-quantitative assessment of the calcareous nannofossil assemblage.

Finally, scanning electron microscope (SEM) images of bulk samples and microfossils used for isotopic measurements were obtained at the Earth Sciences Department of the University of Turin using a JEOL JSM IT300LV. Images were used to assess the preservation and abundance of microfossils, with a focus on the Lago-Mare interval.

3.5. Stable isotopes

The oxygen ($\delta^{18}O$) and carbon ($\delta^{13}C$) stable isotopic composition of selected species of planktonic foraminifera (*Orbulina universa*, *Globigerinoides obliquus* and *Globigerinoides extremus*) and ostracods (*Cyprideis* and *Loxocorniculina djafarovi*) were performed using a *Thermo 253, Thermo GasBench II* coupled to a *Thermo 253* isotope ratio mass spectrometer in continuous flow mode, thermostatic sample tray and a *GC PAL* autosampler at the Goethe University–Senckenberg BiK-F Joint Stable Isotope Facility in Frankfurt. Over the measurements, analytical precision was 0.07‰ for $\delta^{18}O$. Results are reported against Vienna Pee Dee Belemnite (VPDB) using the standard δ notation expressed in per mil (‰).

Before isotope analyses, for each selected foraminifera and ostracod species, a minimum of ~100 μg was hand-picked from the pre-cleaned fraction that was first sonicated in MeOH for about 10 s to remove adhered matrix particles, further rinsed five times in MilliQ water and finally dried in clean hoods under constant airflow. To avoid reworked extinct species contaminating the Lago-Mare interval, *Orbulina universa* and Globigerinoides obliquus planktonic foraminifera were selected for subsequent SSS calculation. Among ostracods, based on their preservation, abundance and occurrence, *Loxocorniculina djafarovi* and *Cyrideis* spp. were selected from the Lago-Mare sediments, whereas *Cyprideis* spp. (Maccarone and Pollenzo sections) and *Agrenocythere* spp. (Stirone section) were selected from the Zanclean (Pliocene).

3.6. SSS estimates using SST and foraminifera $\delta^{18}O$

Planktonic foraminifera calcite oxygen isotopic composition ($\delta^{18}O_{Cc}$) can be used to estimate past changes in salinity because the ambient oxygen isotopic composition of seawater ($\delta^{18}O_{SW}$) in which the shell precipitated co-varies linearly with sea surface salinity (SSS) and temperature (SST) (e.g., LeGrande and Schmidt, 2006). The $\delta^{18}O_{SW}$ and SSS increase with evaporation and decrease by addition of freshwater with low-$\delta^{18}O$ values. Based on this concept and like earlier studies (e.g., Antonarakou et al., 2015; Kontakiotis et al., 2019; Vasiliev et al., 2019; Kontakiotis et al., 2022), we used a multiproxy geochemical approach to estimate regional past SSS variability at the MZB in the Northern Mediterranean. To estimate the $\delta_{18}O_{SW}$ from the measured foraminiferal $\delta^{18}O_{Cc}$ values, the temperature component was removed using the *Orbulina universa* low-light paleotemperature equation of Bemis et al. (1998):

$$T = 16.5\text{–}4.80 \times \left(\delta^{18}O_{Cc}\text{–}\left(\delta^{18}O_{SW}\text{–}0.27‰\right)\right) \ (\pm 0.7°C) \quad (5)$$

Eq. (5) has been initially calibrated for a temperature range between 15 and 25 °C but was then used with good results in warmer waters as those reconstructed into the Mediterranean during the Late Miocene and Early Pliocene (Kontakiotis et al., 2019; Bulian et al., 2022). The salinity is obtained by removing temperature from the $\delta^{18}O$ record using the equation by Bemis et al. (1998). To correct the equation for the continental ice volume effect, we used the Late Miocene and Early Pliocene records of eustatic sea level changes as modelled by Miller et al. (2011). We linearly interpolated the Miller et al. (2011) record for the studied time period and generated a record of global $\delta^{18}OSW$ change over the upper Miocene to lower Pliocene transition by converting the sea-level data into mean ocean $\delta^{18}O$ changes and applying a 0.008 ‰ increase per meter of sea-level lowering (Siddall et al., 2003). Then, we subtracted this component from the $\delta^{18}OSW$ profile to obtain the regional ice volume free $\delta^{18}OSW$ ($\delta^{18}O_{IVF\text{-}SW}$) as described earlier (Kontakiotis et al., 2022). The calculated $\delta^{18}O_{IVF\text{-}SW}$ values are a function of changes in regional hydrography. Therefore, these $\delta^{18}O_{IVF\text{-}SW}$ are considered to approximate local variations in SSS (Kontakiotis et al., 2022). Absolute errors in $\delta^{18}O_{IVF\text{-}SW}$ were considered insignificant for the Late Miocene since changes in global ice volume were small (Williams et al., 2005). To convert the $\delta^{18}O$ signal to absolute SSS values we used the modern $\delta^{18}O_{sw}$–salinity relationship for the Mediterranean Sea: $\delta^{18}O = 0.25 \times S - 8.2$ (Pierre, 1999).

4. Results

4.1. The $C_{37:4}$[%] and the C_{37}/C_{38} ratio

A suite of LCA with carbon numbers ranging from 37 to 39 was identified in the studied sections (supplementary Table S2). Whereas C_{39} was found in low concentrations, C_{37} and C_{38} are more abundant, but in varying proportions (supplementary Table S2; Fig. S4). Similarly, also the C_{37} group of isomers shows significant variation (see supplementary Table S2 and Fig. S5). Only in three samples (MC2.1, MC2.3, ST10.7), LCA were not found and the $C_{37:4}$[%] and the C_{37}/C_{38} ratio were not calculated.

In the Maccarone section (Fig. 3), the $C_{37:4}$[%] index is continuously decreasing from the lowermost sample (15.2%) to the col2 (0.4%) (Fig. 3A).

The overall decreasing trend is interrupted in the DL2 above col3, where $C_{37:4}$[%] is increasing to 13.3%. After this single peak, the values are generally below 5.0% in both the uppermost Messinian and Zanclean sediments, except for one sample just above the Miocene-Pliocene boundary (Fig. 3A). In contrast, the C_{37}/C_{38} ratio (Fig. 3B) oscillates between 0.5 and 1.7, without any trend.

In the Stirone section (Fig. 4), the $C_{37:4}$[%] index is constant with values around 2.0% in the Messinian interval until the DL3, where the value increases up to 6.9%. Above the DL3, in the Zanclean sediments, values dropped to <0.5% (Fig. 4A). The variation of the C_{37}/C_{38} ratio is close to 1 both in the Messinian and Zanclean intervals, except for two levels just below and within the DL3, where values close to 3 are observed (Fig, 4B).

In the Pollenzo section (Fig. 5) the $C_{37:4}$[%] index of the Messinian interval is always >5.0% and increases from bottom to midpoint to a maximum value of 23.4% at 200 cm; above the DL3, in the Zanclean interval, the $C_{37:4}$[%] decreases to values <1% (Fig. 5A). The C_{37}/C_{38}

ratio in the Messinian interval is characterized by values >1 (Fig. 5B), with two peaks at the bottom of the section (2.0%) and within the DL3 (1.9%); in the Zanclean interval the C_{37}/C_{38} values are constantly <1 (Fig. 5B).

4.2. Micropaleontology

4.2.1. Foraminifera

In the Messinian sediments, common foraminifera are exclusively observed at Maccarone section (supplementary Table S1) where they present lower abundances compared to the Zanclean interval. Additionally, the scarce foraminifera of the Lago-Mare interval consist of a mixture of long-ranging taxa (e.g., *Globigerina bulloides*, *Orbulina universa*, *Globigerinoides obliquus* and Globi*gerinoides extremus*) and reworked species from the Early Miocene (*Paragloborotalia mayeri*, *P. semivera, P. acrostoma, P. pseudokugleri* and Cata*psydrax dissimilis)*. Among the long-ranging taxa*, O. universa* and *G. obliquus* are quite rare and only occur in a few levels (at 460 and 1020 cm and 460, 800, 950 and 1020 cm, respectively). SEM observations allow the recognition of well-preserved and pristine microcrystalline calcite of the wall of both reworked and long-ranging taxa. In the Stirone and Pollenzo sections only small-sized and uncommon globigerinids, often fragmented, occurs. In contrast to the Messinian sediments, foraminifera in the Zanclean sediments are present in all sections with a well (Stirone and Pollenzo) to moderate (Maccarone) preservation. In Pollenzo and Maccarone, the typical Early Zanclean bioevents (Lirer et al., 2019) were recorded, including two coiling shifts of left-coiled *Neogloboquadrina acostaensis* (Maccarone 1st at 1045 cm and 2nd at 1095 cm, Pollenzo 1_{st} at 430 cm and 2nd at 500 cm), the re-appearance of the benthic foraminifera *Siphonina reticulata* (Maccarone at 1275 cm) and the acme of *Sphaeroidinellopsis* spp. (Maccarone at 1095 cm). *Globorotalia margaritae* was only observed in the Stirone section from 5 cm above the DL3.

4.2.2. Ostracods

In the Maccarone section, fragmented and prevalently adult disarticulated valves of the typical Lago-Mare ostracod assemblage (see Grossi et al., 2008) were observed in the Messinian sediments (supplementary Table S1). Only sparse adult valves of *Cyprideis* were instead observed in some Zanclean samples (at 1045, 1135, 1275, 1355 and 1395 cm). In Stirone and Pollenzo, the ostracod assemblages of the Lago-Mare intervals are similar to those of the Maccarone section, but in both sections, juvenile and adult valves coevally occur. Marine ostracods (*Agrenocythere* spp.) were common in the Zanclean sediments only in the Stirone section (at 1430, 1460, 1480 and 1560 cm). As for foraminifera, SEM observations indicate that the calcitic ostracod valves were well preserved (supplementary Table S1).

4.2.3. Calcareous nannofossils

Calcareous nannofossils (CN) were found in both Zanclean and Messinian sediments, with an overall lower abundance in the latter interval (supplementary Table S1). Reworked taxa, such as *Cyclicartolithus* spp. (Eocene to Middle Miocene), are quite common in the Messinian sediments and decrease with sedimentation rates, above the col3 in the Maccarone section and the MZB in all the sections (supplementary Table S1). SEM observations indicate that the preservation of CN is generally good and does not vary significantly across the MZB; coccospherae are observed in both Messinian and Zanclean sediments, and *Reticulofenestra* gr. are commonly present in all the samples representing the most abundant taxon among the CN assemblage (supplementary Table S1).

In the Messinian interval of the Maccarone and Pollenzo sections, *Reticulofenestra minuta* is more frequently observed than other larger taxa, such as *R. haqii* and *R. antarctica* that are more common during the Zanclean. *Coccolitus pelagicus*, *Sphaenolitus* spp. and *H. carteri* were also observed in the samples, with no obvious relation with the stratigraphy (supplementary Table S1). SEM and optical microscope observations suggest that above col3, the CN assemblage is more diversified than below (supplementary Table S1).

4.3. $U^{k'}_{37}$ based SST

Based on the $U^{k'}_{37}$ values described in supplementary Table S2 we calculated the corresponding SST using the calibration by Conte et al. (2006). In Maccarone, the SSTs values (Fig. 3C) are higher than 20 °C in the lowermost sample, just below the DL1. After a slight decrease to 16 °C at 460 cm, the SSTs increase again up to col3, reaching the highest values of the record (28 °C). After that, the lowest value (14 °C) is recognized between DL2 and DL3, which preludes a second increase up to the DL3 (20 °C), followed frequent and large variations between 18.0 and 25.5 °C in the lowermost Zanclean interval. For the rest of the Zanclean, the fluctuations range between 15.0 and 21.2 °C and occur at a lower frequency, in an interval characterized by lower sample resolution.

At Stirone (Fig. 4C), Messinian SSTs decrease from 24.8 to 7 °C just below the DL3. The DL3 displays increasing temperatures above 20 °C, which persisted also in the Zanclean at around 25 °C.

In the Pollenzo section, the SST values (Fig. 5C) of the Messinian interval increase from 9.3 °C to 11.9 °C just below the MZB; then, the SST rapidly increases to 24.4 °C in the DL3. Similar values typify the Zanclean interval (22.6 to 25.8 °C), showing no relevant fluctuations.

4.4. Calcareous microfossil $\delta^{18}O$ and SSS estimates

The $\delta^{18}O$ values of planktonic foraminifera of the Maccarone section (Fig. 3D) are −1.2 to −0.2‰ for *O. universa*, −1.2 to −0.4‰ for *G. obliquus* and − 1.3 to −0.4 ‰ for *G. extremus*. The most negative values were measured for the Globigerinoides specimens in the interval between the col3 layer and the DL3 of the Maccarone section (Fig. 3D; supplementary Table S2). Similar values were also recorded in the topmost Zanclean sample for the three species. Values measured in *O. universa* are mostly from Zanclean sediments and display higher variability than those of the two *Globigerinoides* species. Ostracods, which are represented by *Cyprideis* (Messinian and Zanclean intervals) and L. *djafarovi* (only Messinian), show values that range from −1.9 to +0.4‰ and from −2.1 to −1.1‰, respectively (Fig. 3D). Cyprideis valves show light values very similar to those of L. *djafarovi* in the Messinian interval and values close to zero in the Zanclean interval, with a marked shift towards more positive values across the MZB.

In the Stirone section, no foraminifera were found in the Messinian interval (Fig. 4D, supplementary Table S2), and $\delta^{18}O$ data were obtained only for the Zanclean interval. The $\delta^{18}O$ values of *O. universa* range from +0.6 to +1.0‰, whereas those of *G. obliquus*, are lighter, ranging from −1.4 to +0.5‰. The $\delta^{18}O$ of Messinian *Cyprideis* valves increases from −0.9‰ at the bottom of the section to +1.9‰ at the top of the DL3, with a marked increase within the DL3. The $\delta^{18}O$ of *Agrenocythere* in the Zanclean sediments decreases from +2.3‰ at the top of the DL3 to values around +1.3‰ at the top of the studied interval (Fig. 4D).

In the Pollenzo section, the $\delta^{18}O$ record of planktonic foraminifera (Fig. 5D, supplementary Table S2) is limited to the Zanclean interval, with values ranging between −1.0 and + 0.7‰ for *O. universa* and between −1.6 and − 0.6‰ for *G. obliquus*. Among the values measured on ostracods, *Cyprideis* have a negative $\delta^{18}O$ value of −0.4‰ in the Messinian sample FFS4 (300 cm); then, in the Zanclean deposits the two datapoints have a positive (+0.9‰) and a negative (−1.0‰) value as measured on fragmented *Cyprideis* valves.

When combining the SSTs and the $\delta^{18}O$ of foraminifera, the reconstructed SSS values show that at the Maccarone section, the Zanclean SSS varies from 32.4 PSU to 37.4 PSU, with an average of 34.3 PSU (Fig. 3E), while in the Pollenzo section the Pliocene SSS ranges from 34.8 PSU to 35.9 PSU, with an average of 35.8 PSU (Fig. 5E). In the Stirone section, salinity values into the Pliocene range between 36.3 and 41.0 PSU (Fig. 4E).

For the Messinian interval, SSS was only calculated for four samples of the Maccarone section using both *O. universa* and *G. obliquus* and SSS ranges from 32.8 PSU to 36.2 PSU (Fig. 3E).

5. Discussion

5.1. Paleoenvironmental reconstruction based on long-chain alkenones

In all the studied sections, the Zanclean sediments are characterized by very low C_{37}/C_{38} ratios and $C_{37:4}$[%] (Fig. 6A), which are typical for LCA of Group III (Longo et al., 2016). Group III is represented by the coccolithophorids *E. huxleyi* or *G. oceanica* (Fig. 6A), thriving in modern marine environment. In fact, in modern seas, these species are characterized by C_{37}/C_{38} values <3 and $C_{37:4}$[%] ranging from 0 to 9% (increasing with decreasing temperature; Chu et al., 2005; Wang et al., 2015). Interestingly, the common occurrence of the coccolithophorid *Reticulofenestra* gr. in the lowermost Zanclean sediments, which is considered as an ancient representative of *E. huxleyi* (Beltran et al., 2011; Athanasiou et al., 2017) (supplementary Table S1; Note S3) supports the marine origin of the LCA in the Zanclean. The Zanclean marine LCA signature is further confirmed by the presence of a diversified assemblage of calcareous planktonic and benthic microfossils, indicating an open marine paleoenvironment (Iaccarino and Papani, 1979; Gennari et al., 2008; Bulian et al., 2022), in agreement with other observations from this time interval in the Mediterranean (Spezzaferri et al., 1998; Iaccarino et al., 1999; Di Stefano and Sturiale, 2010; Vasiliev et al., 2017; Bulian et al., 2022).

In contrast, the values of the Messinian LCA-proxies are more scattered (Fig. 6A) and form distinct clusters for each studied section. In Maccarone, the C_{37}/C_{38} values (1.5–0.5) are low, but the variation of the $C_{37:4}$[%] is larger (0.4–15%), with values higher than that expect for marine LCA signature, especially in the lower part of the section (up to

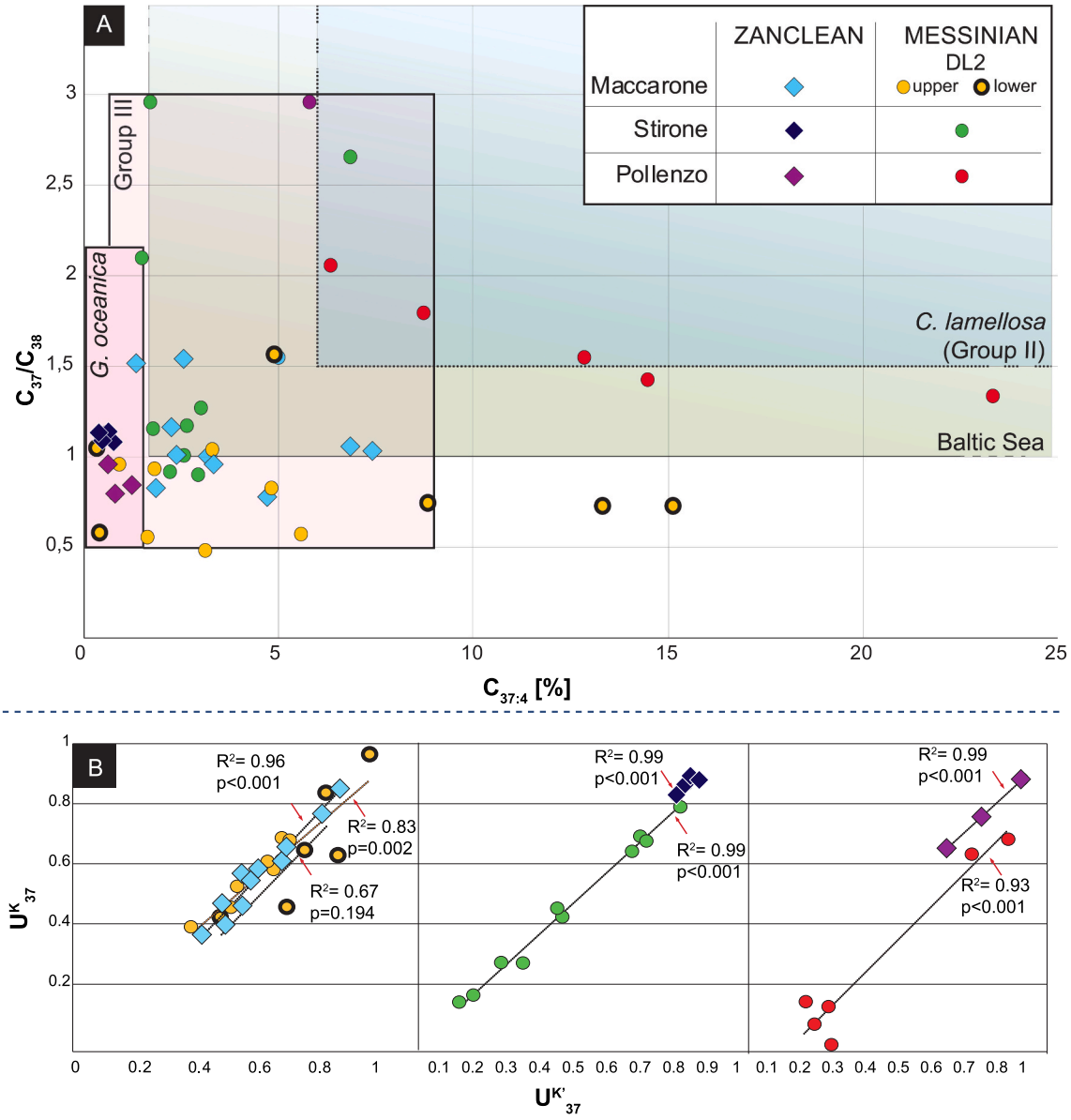

Fig. 6. (A) Cross plot of the long chain alkenone (LCA) C37/C38 ratio versus LCA C37:4[%]. Rectangles border the typical ranges of Group II (*C. lamellosa*) and III (marine) LCA producers (Chu et al., 2005; Wang et al., 2015), and of *G. oceanica* (Chu et al., 2005; Wang et al., 2015). The green area encloses part of the ranges of LCA producers of the Baltic Sea (Chu et al., 2005; Wang et al., 2015); (B) Cross plots with the linear correlation between U^{k}_{37} and Uk'_{37} ($U^{k'}_{37}$/ U^{k}_{37} ratio). p is the Pearson coefficient which measures the strength of the linear relationship between two variables; R^2 represents the proportion of one variable's variance that can be explained by the variance in another variable in a linear regression model. (For interpretation of the references to colour in this figure legend, the reader is referred to the web version of this article.)

DL2; Fig. 6A). Such a LCA distribution (low C_{37}/C_{38} and high $C_{37:4}$[%]) has no known modern analogue. Whereas low C_{37}/C_{38} values are also characteristic of hypersaline lakes, the higher $C_{37:4}$[%] values (up to 15%;) are rather in line with brackish or freshwater environments (Chu et al., 2005 and references therein). Considering that marine and brackish LCA may have the same C_{37}/C_{38} ratios, this signature can potentially derive from a mixture of an (unknown) Messinian analogue of the brackish haptophyte *C. lamellosa*, responsible for the increase of $C_{37:4}$[%] in relatively warm surface waters, and of marine producers, with lower $C_{37:4}$[%]. The relatively low correlation coefficient and significance ($R^2 = 0.67$, $p = 0.194$; Fig. 6B) between the $U^{k'}_{37}$ and U^{k}_{37} in this interval supports the presence of a weak correlation due to the mixing of different contributors to the overall LCA pool.

In great contrast, from the base of col3 up to the DL3, the Messinian LCA signature is indistinguishable from that of the marine Zanclean sediments, and the correlation coefficient of the $U^{k'}_{37}$ /U^{k}_{37} ratio is consistently higher (Fig. 6B; $R^2 = 0.83$, $p = 0.002$) in Messinian and $R^2 = 0.96$, $p < 0.001$ in the Zanclean). This possibly suggests that in the Maccarone section, the latest Messinian LCA were progressively sourced by marine coccolithophorids of Group III.

The Messinian Stirone samples are clustered in the field of the modern marine Group III (Fig. 6A) with a rather constant source of LCA, as suggested by the high correlation coefficient between $U^{k'}_{37}$ and U^{k}_{37} ($R^2 > 0.99$, $p < 0.01$; Fig. 6B). However, the co-occurrence of Group II brackish producers in some of the layers (from 8.35 m to 12.65 m and at the MZB) is possible, as displayed by the C_{37}/C_{38} values >1.6 (Fig. 6A).

Finally, the Messinian Pollenzo samples are typified by relatively high $C_{37:4}$ [%] and C_{37}/C_{38} values, which closely reflect the *C. lamellosa* (Group II) signature, indicative of coastal marine environments and brackish waters (Chu et al., 2005; Wang et al., 2015; Huang et al., 2021), and by a high $U^{k'}_{37}/U^{k}_{37}$ correlation coefficient ($R > 0.99$, $p < 0.001$) pointing to a uniform source of LCA.

5.2. Orbital forcing on SST fluctuations and age model

The abundant presence of marine LCA in most of the Lago-Mare and Zanclean sediments of the studied sections allowed the reconstruction of SST using the calibration of the degree of unsaturation state of LCA ($U^{k'}_{37}$) of Conte et al. (2006). For the Messinian sediments, abundant LCA sourced from Group II (possibly representing an analogue of *C. lamellosa*) are likely responsible for the very cold SST values recorded in the Pollenzo section. Such a bias possibly reflects the different correlation of the degree of LCA unsaturation with temperature for Group II and Group III (Wang et al., 2015). Anyway, the general trend of SST values is similar between the three sections and mirrors the insolation trend (Fig. 7), without significant differences between environments characterized by predominantly marine (Maccarone) or brackish (Pollenzo) LCA. In the Messinian interval, the pattern of these fluctuations implies that relatively warmer SSTs are achieved in or close to the col3 layers and at the MZB; in the Maccarone section only, another interval of relatively warm SSTs occurs close to the DL2, just above the col2 (both not sampled in our section; see Figs. 1B; 3). This is of interest since the Colombaccio layers and the MZB were previously tuned to consecutive 65°N summer insolation maxima at 5.37 Ma (col2), 5.35 Ma (col3) and 5.33 Ma (MZB), applying cyclostratigraphy, physical stratigraphy (Roveri et al., 2006; Roveri et al., 2008a) and biomagnetostratigraphy (Van Couvering et al., 2000; Gennari et al., 2008).

The tight correspondence between 65° N insolation maxima and

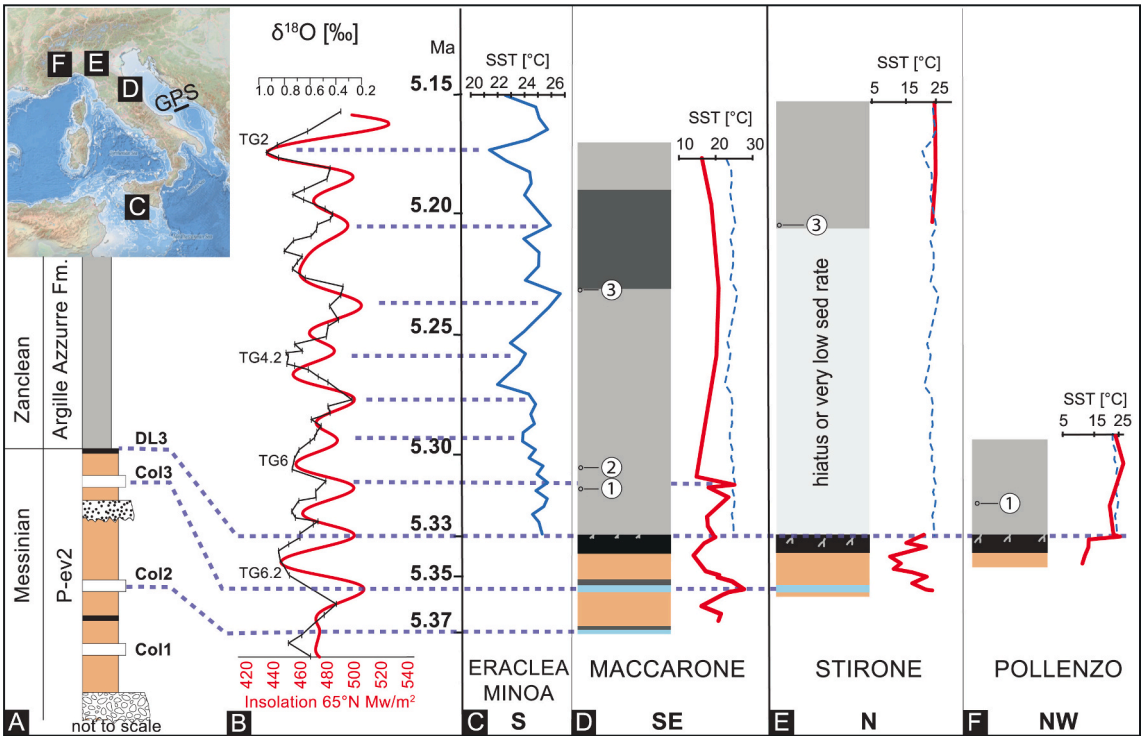

Fig. 7. Astronomical tuning and cyclostratigraphic correlation of the studied sections (not to scale). A) Northern Mediterranean reference section (Gennari et al., 2008); and geographic map of Italy with the location of study and Eraclea Minoa sections, GPS indicates the location of the Gargano-Pelagosa sill (Pellen et al., 2017); B) the reference $\delta^{18}O$ oceanic curve of Van der Laan et al. (2006) (black), the insolation curve of Laskar et al. (2004) (red) and the marine isotopic glacial stages cited in the text (TG 6.2, 6, 4.2 and 2) are indicated. C) SST trend for the Eraclea Minoa Zanclean GSSP reference section (Herbert et al., 2016); the same values are plotted in D, E and F (blue dotted lines), for comparison with SST reconstructions for the studied section. D) Maccarone SST record (red line); E) Stirone SST record (red line); F) Pollenzo SST record (red line). Col1, Col2 and Col3 are the Colombaccio layers of Bassetti et al., 2004; DL3 is the dark layer associated to the MZB. Biostratigraphic events used to correlate the study section with the Eraclea Minoa section are: 1) the first influx of left coiled *Neogloboquadrina acostaensis* (5.31 Ma); 2) the second the first influx of left coiled *N. acostaensis* (5.29 Ma) and 3) the reappearance of *Siphonina reticulata* (5.20 Ma) (Gennari et al., 2008; Lirer et al., 2019). (For interpretation of the references to colour in this figure legend, the reader is referred to the web version of this article.)

warm SSTs strongly suggests that the insolation is the driver of temperature increase in the Messinian interval. Accordingly, the lower SST values derived for the intervals in-between the col2 to col3 and col3 to DL3 intervals most likely record two successive insolation minima. Among these two insolation minima, the relatively cooler value corresponds to the glacial isotopic stage TG6.2, dated at ca. 5.34 Ma (Van der Laan et al., 2006).

Biomagnetostratigraphic data (Gennari et al., 2008) allowed a straightforward correlation of the lowermost Zanclean interval in all three studied sections, reinforcing the assumption that the Zanclean SSTs in the Mediterranean Basin were also strongly forced by insolation. The LCA-based orbital pattern obtained here was not documented in the Eraclea Minoa section (Herbert et al., 2016), located at more southern latitudes, although insolation-related lithological cycles occur also there. In our study, Northern Mediterranean SSTs of insolation minima are on average 3 to 7 °C lower than those calculated by Herbert et al. (2016) for the Eraclea Minoa site. For insolation maxima, SSTs of both northern and southern sites are comparable. The strong SSTs difference during insolation minima suggests a stronger latitudinal gradient during insolation maxima, similarly to the increased SST gradient between mid and low-latitude oceans during the Last Glacial Maximum (Trend-Staid and Prell, 2002). Due to a lower sample resolution in the upper part of Maccarone with respect to the corresponding interval of Eraclea Minoa, the comparison between SSTs at insolation minima and maxima between 5.308 and 5.178 Ma is not possible. Overall, the integration of SST reconstructions with biostratigraphic data for the Zanclean (Van Couvering et al., 2000; Iaccarino and Papani, 1979; Gennari et al., 2008) and the post-evaporitic Messinian supports the correlation of the studied sections with the insolation curve (Fig. 7) (Roveri et al., 2008a).

In summary, the Maccarone section includes the oldest studied sediments dated at ca. 5.37 Ma (the age of col2), which corresponds to a period of relatively high SSTs.

The col3 layer (and associated warms SST) is recorded in the Maccarone section and at the base of the Stirone section and is dated at ca. 5.35 Ma. The Messinian portion of the Pollenzo section is dated and correlated to the other two sections by means of the low SST corresponding to the prominent isotopic glacial stage (TG 6.2; 5.34 Ma) and the warm MZB. The age model and the correlation of the three sections allow the comparison of the sedimentation rates, which change from higher to lower values at the MZB in the Stirone (Fig. 4F) and Pollenzo (Fig. 5F) sections. In the Maccarone section, a similar change is observed instead just above the col3 layer (Fig. 3F).

5.3. Marine microfossils in the Lago-Mare sediments of the Northern Mediterranean: reworked or not?

The debate about the prevailing paleoenvironmental conditions during the Lago-Mare phase in the Mediterranean is still ongoing (see Andreetto et al., 2021). In the northern Mediterranean, the Lago-Mare deposits were originally attributed to relatively shallow (few tens of meters deep) fresh to brackish water environments, mostly based on the shallow-water ostracod assemblages (e.g., Grossi et al., 2008).

Marine microfossils (foraminifera, calcareous nannofossils and dinocysts) were recognized in the Mediterranean Lago-Mare sediments, including those of the Maccarone and Stirone sections, but they were considered as reworked (Iaccarino and Papani, 1979; Roveri et al., 2008c; Grossi et al., 2008; Stoica et al., 2018; Grothe et al., 2018). The reworking was proposed because of the presence and abundance of extinct species of pre-Lago-Mare ages, the varying preservation and, regarding foraminifera, the small size and sorting (Grossi et al., 2008; Grossi and Gennari, 2008; Roveri et al., 2008a; Andreetto et al., 2022a). However, allegedly in-situ marine calcareous nannofossils (the source of Group III LCA) were observed in the Lago-Mare sediments in Maccarone (Popescu et al., 2017), and Pollenzo (Andreetto et al., 2022a), suggesting that this marine group inhabited, at least temporarily, this part of the Mediterranean well before the base of the Zanclean.

Indeed, our LCA data indicate that, sporadically, coccolithophorids inhabited the Lago-Mare environment(s) of the Northern Mediterranean at least since 5.37 Ma at Maccarone, and more consistently from 5.35 Ma at Stirone, as well. Such inference agrees with SEM observations (Supplementary Note S3), showing the common presence of intact coccospheres already in the Lago-Mare sediments of the Maccarone and Stirone sections, beginning from above the col3 layers (5.35 Ma). This challenges the freshwater to oligohaline salinities reconstructed for this specific Lago-Mare interval (Grossi et al., 2008; Pellen et al., 2017), based on ostracods. Specimens of this group indeed display a well-preserved wall structure in both sections, but the valves are mostly broken, and juvenile specimens are absent (see also Mancini et al., 2023), suggesting downslope transport from more marginal settings.

In contrast, intact valves and the presence of juvenile specimens in the Pollenzo section suggest that Lago-Mare ostracods are in situ (Andreetto et al., 2022a), which points to a shallow and oligohaline paleoenvironment in line with the dominance of Group II LCA (C. lamellose-type). However, both SEM observations and the LCA signature of the sediments indicate that coccolithophorids were also present in the northernmost Pollenzo location, although in smaller proportion than in the southern Stirone and Maccarone sites (see also Andreetto et al., 2022a). The widespread record of coccolithophorids in the three sections under different paleoenvironmental conditions can also be attributed to their adaptability to brackish conditions, as found in the modern Black Sea (salinity 16-19 PSU; Giunta et al., 2007) and the marginal Adriatic Sea (16.9-35.3 PSU; Skejić et al., 2021). In particular, in the Pollenzo section the uppermost Messinian sediments are typified by diverse Paratethyan ostracods, mixed with calcareous nannofossils and dinocysts adapted to brackish environments (Andreetto et al., 2022a). This peculiar assemblage, recorded by both body fossils and LCA, and the $^{87}Sr/^{86}Sr$ ratio of ostracods (Andreetto et al., 2022a) may agree with a mixture of Mediterranean, Paratethyan and Atlantic waters, typical of the Lago-Mare phase.

In contrast to the more versatile coccolithophorids, planktonic foraminifera exclusively inhabit marine waters; thus, the brackish conditions, which were revealed by variable amounts of LCA representatives of Group II, suggest that the small-sized and fragmented specimens of planktonic foraminifera observed in the Lago-Mare sediments of Pollenzo and Stirone are indeed reworked. At Maccarone, the foraminifera assemblage includes common Early Miocene extinct taxa and the scarcity/absence of *O. universa*, a common Middle Miocene to recent species, suggests that foraminifera were reasonably reworked from Early Miocene sediments. Only in three layers *O. universa* co-occurs with long-ranging Late Miocene to Pliocene taxa (*Globigerinoides obliquus*) (Fig. 3). Such an assemblage is possibly in situ and could indicate occasional influxes of more saline waters. The SSS calculated for these levels would indicate normal to slightly lower than normal marine salinities (in comparison to those reconstructed for the Zanclean interval), consistent with our paleoenvironmental reconstruction (Fig. 3; supplementary Table S2).

5.4. The Northern Mediterranean at the end of the MSC

Changes of the LCA assemblage in the investigated sections reflect salinity fluctuations in surface waters of the northern Mediterranean basin from the latest Messinian (5.37 Ma) to the early Zanclean. The new dataset and the astronomical dating of the three sections allow tracking the temporal and spatial paleoenvironmental modifications along a SE-NW transect, from the main Northern Apennine foredeep (Maccarone) to the northernmost sector of the Mediterranean (Pollenzo), passing through a marginal wedge top basin (Stirone).

In the SE area (Maccarone section), during the 5.37-5.35 Ma time interval, surface waters were inhabited by brackish and marine LCA producers, probably dwelling in a mesohaline environment (Fig. 8A). Fully freshwater conditions (Grossi et al., 2008; Pellen et al., 2017) are unlikely, due to the absence of LCA values typical of Group I (Fig. 6),

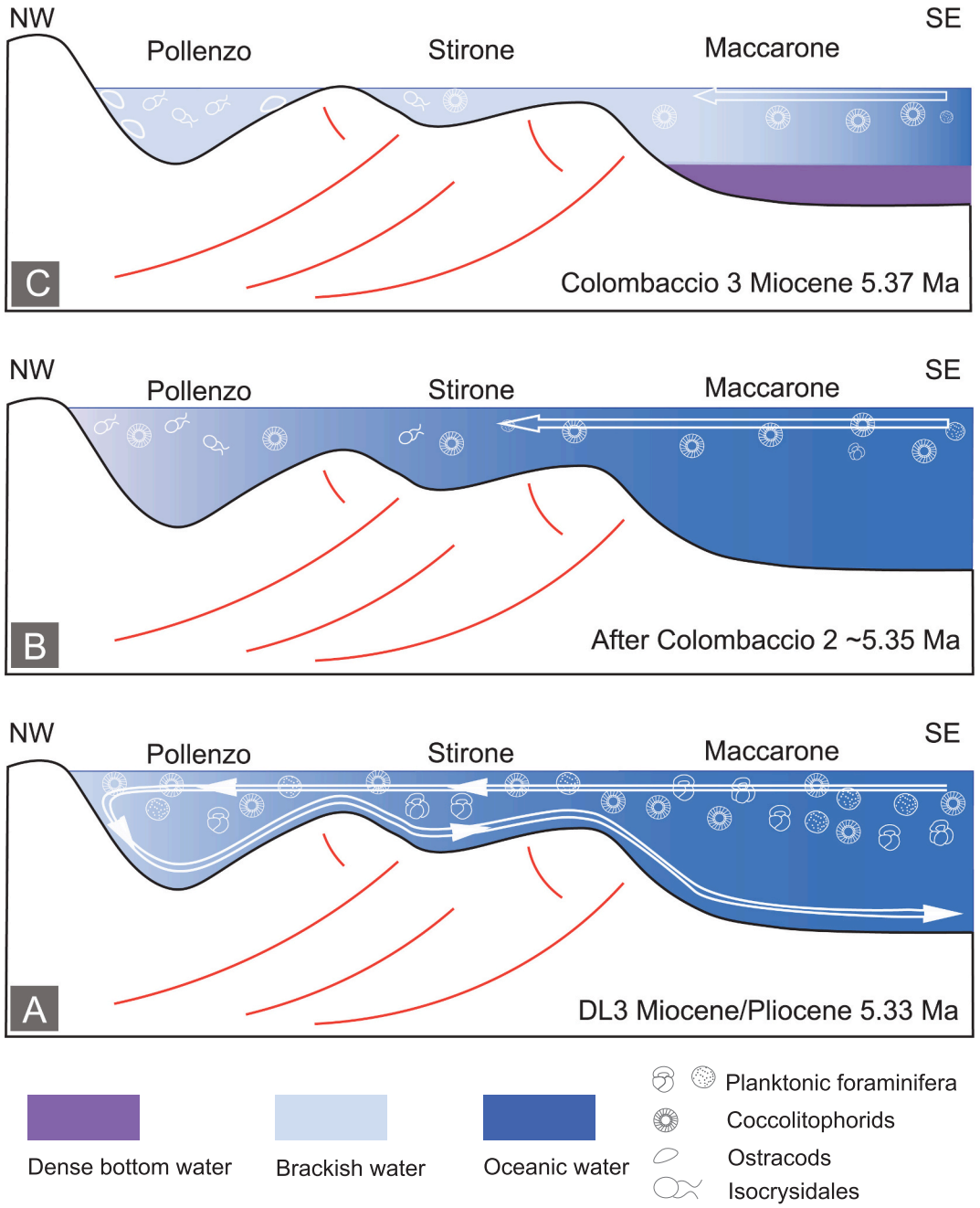

Fig. 8. Schematic reconstruction of the stepwise paleoenvironmental conditions in the Northern Mediterranean between 5.37 Ma and the Early Zanclean (from A to C, see text for details). The blue arrows indicate the input of the more saline oceanic water into the Northern Mediterranean; the white arrows indicate the recovery of the Mediterranean antiestuarine circulation after the MZB. (For interpretation of the references to colour in this figure legend, the reader is referred to the web version of this article.)

whereas episodic influxes of marine waters are suggested by the sporadic occurrence of in situ planktonic foraminifera (supplementary Table S2; *Orbulina universa* and *Globigerinoides* spp.) and marine dinocysts (Pellen et al., 2017).

Between 5.35 and 5.33 Ma (Fig. 8B), a shift towards marine conditions (predominance of Group III LCA) is recorded in the main foredeep. Such a shift agrees with the "quasi-marine" $\delta^{18}O$ signature (Bassetti et al., 2004) of the col3 layer, compared to the more negative $\delta^{18}O$ values of the older col2 layers (see Bassetti et al., 2004). Planktonic foraminifera are still sporadic and indicative of low salinity marine waters. However, moving to the more marginal central and NW sectors, the environment is gradually more influenced by brackish waters, as indicated by the different LCA clustering at Stirone and by the dominance of Group II LCA in the Pollenzo section. Another evidence of transient marine connections into the northern Mediterranean basin during the Lago-Mare phase is the presence of in-situ marine fish remains and otoliths (Carnevale et al., 2006, 2008, 2018, 2019; Schwarzhans et al., 2020). This supposedly well-connected basin was still influenced by a strong regional salinity gradient from SE to NW in surface waters. Normal marine salinity was reached in the main Apennine foredeep (Maccarone section), which represented a more open setting, less influenced by runoff and closer to the marine water body source, possibly located to the south of the recently identified Pelagosa Gargano sill (Pellen et al., 2017). In contrast, brackish conditions still characterized the northern domain (Stirone and Pollenzo sections) which was far away from the sill and more affected by the influx of

freshwater from rivers (Fig. 8B). This lateral transition towards more brackish environments is also indicated by the negative $\delta^{18}O$ values of shallow water ostracods in all the sections during the 5.35-5.33 Ma interval (Figs. 3D, 4D, 5D). Noteworthy, only in the Stirone and Pollenzo sections these ostracods are in situ, whereas in the distal Maccarone section they were transported and are thus representative of more coastal waters.

In summary, the use of LCA as a paleoenvironmental proxy suggests that the demise of the MSC in the northern Mediterranean basin was caused by the gradual and probably stepwise replacement of brackish water by marine water from the southern and distal setting (as early as 5.37 Ma) to the northern and more marginal ones (since 5.35 Ma). A salinity gradient was most likely present until 5.33 Ma; later on, marine conditions were re-established in all the basins (Fig. 8C). At that time, a positive excursion (+1‰) of the $\delta^{18}O$ values of the ostracods is indicative of increasing salinity also in the more marginal portions of the basin; since SST data indicate a warming across the MZB, the role of temperature on such isotopic excursion is unlikely (Figs. 3, 4, 5). This reconstruction agrees with the backstepping architecture of the post-evaporitic succession of the proto-Adriatic basin (Roveri et al., 2014a, 2014b, 2014c, 2008a), which suggests a stepwise base level rise possibly starting as early as 5.42 Ma (Roveri et al., 2008a). Similar conclusions were drawn by Marzocchi et al. (2016), who suggested a one-way stepwise refilling of the Mediterranean with the Atlantic, explaining the presence of both marine and freshwater fossils after the acme of the MSC. The gradual refilling of the basin is hardly reconcilable with a scenario involving the sudden, catastrophic flooding of the Mediterranean at the end of the MSC (Garcia-Castellanos et al., 2009; Micallef et al., 2018; Amarathunga et al., 2022; Camerlenghi, 2022).

The gradual one-way influx of Atlantic waters into the Mediterranean would have been able to: 1) allow the proliferation of Group III LCA producers and sporadic foraminifera under conditions that were slightly less salty than normal marine; 2) weaken the low saline lid responsible for the stratification of the Mediterranean water column during the Lago-Mare phase (Marzocchi et al., 2016). The weakening of the stratification and its final disruption was induced by the re-establishment of a two-way connection (anti-estuarine circulation) with the Atlantic, which is most likely recorded by the deposition of the dark layer (DL3) at the MZB. Starting from the base of the Zanclean, the whole Mediterranean was recolonized by remarkably diverse communities of marine stenohaline taxa, such as planktonic and benthic foraminifera.

6. Conclusions

Integration of LCA proxies (U^{k}_{37}'/U^{k}_{37}, $C_{37:4}$[%], C_{37}/C_{38} ratio) with micropaleontological data (foraminifera, ostracods, calcareous nannofossils) and independent paleo-salinity estimates (coupled LCA-based SST and $\delta^{18}O$ values of foraminifera) allowed the reconstruction of the paleoenvironmental conditions in the Northern Mediterranean basin at the end of the MSC and across the MZB. The presence of LCA matching with the signature of Group III LCA in the Northern Mediterranean suggests that this branch of the Mediterranean was already receiving influxes from a marine water body before the end of the MSC (at least since 5.37 Ma), most likely through the Pelagosa-Gargano sill. The basin was characterized by strong SE-NW surface salinity gradients, with more saline waters in the south and less saline conditions moving to the north. SST fluctuations were likely controlled by orbital (precessional) cycles. The proposed paleoenvironmental reconstruction agrees with a gradual, one-way, recurring, marine influx-fed base-level rise, causing the progressive replacement of brackish with marine waters already in the latest Messinian and culminating with the re-establishment of fully marine conditions at the base of the Zanclean (5.33 Ma). We consider the dark layer (DL3) just below the first marine Zanclean sediments, as the level where the two-way connection with the Atlantic was established, leading to the complete turnover of the Mediterranean water column. Finally, we stress that LCA-based proxies are an excellent tool for paleoenvironmental reconstructions from sediments characterized by an ambiguous body fossil record, such as those deposited in the Mediterranean during the latest phase of the MSC (Lago-Mare event).

Declaration of Competing Interest

The authors declare that they have no known competing financial interests or personal relationships that could have appeared to influence the work reported in this paper.

Data availability

Data will be made available on request.

Acknowledgments

We thank Sabine Beckmann (University of Hamburg) for support in the lipid biomarker laboratory and Nicole Burdanowitz for sharing some of her alkenone data. FP and IV thank Ulrich Treffert for laboratory support in Frankfurt. This work was supported by University of Turin grants (ex 60% 2021 to Rocco Gennari), the Senkenberg research centre of Frankfurt and the Hamburg Universität. FP was funded from DAAD [grant number: 91818654, 2021]. IV acknowledge support from Deutsche Forschungsgemeinschaft (DFG) - Project number 449448496. We would thank Sarah Feakins and two anonymous reviewers for their valuable feedback and insightful suggestions that contributed to the improvement of this manuscript.

Appendix A. Supplementary data

Supplementary data to this article can be found online at https://doi.org/10.1016/j.palaeo.2023.111831.

References

Aguirre, J., Sánchez-Almazo, I.M., 2004. The Messinian post-evaporitic deposits of the Gafares area (Almería-Níjar basin, SE Spain). A new view of the "Lago-Mare" facies. Sediment. Geol. 168 (1–2), 71–95.

Amadori, C., Garcia-Castellanos, D., Toscani, G., Sternai, P., Fantoni, R., Ghielmi, M., Di Giulio, A., 2018. Restored topography of the Po Plain-Northern Adriatic region during the Messinian base-level drop—Implications for the physiography & compartmentalization of the palaeo-Mediterranean basin. Basin Res. 30 (6), 1247–1263.

Amarathunga, U., Hogg, A.M., Rohling, E.J., Roberts, A.P., Grant, K.M., Heslop, D., Hu, P., Liebr, D., Westerhold, T., Zhao, X., Gilmore, S., 2022. Sill-controlled salinity contrasts followed post-Messinian flooding of the Mediterranean. Nat. Geosci. 15 (9), 720–725.

Andreetto, F., Aloisi, G., Raad, F., Heida, H., Flecker, R., Agiadi, K., Lofi, J., Blondel, S., Bulian, F., Camerlenghi, A., Caruso, A., 2021. Freshening of the Mediterranean Salt Giant: controversies & certainties around the terminal (Upper Gypsum & Lago-Mare) phases of the Messinian Salinity Crisis. Earth Sci. Rev. 216, 103577.

Andreetto, F., Mancini, A.M., Flecker, R., Gennari, R., Lewis, J., Lozar, F., Natalicchio, M., Sangiorgi, F., Stoica, M., Dela Pierre, F., Krijgsman, W., 2022a. Multi-proxy investigation of the post-evaporitic succession of the Piedmont Basin (Pollenzo section, NW Italy): a new piece in the stage 3 puzzle of the Messinian Salinity Crisis. Palaeogeogr. Palaeoclimatol. Palaeoecol. 594, 110961.

Andreetto, F., Flecker, R., Aloisi, G., Mancini, A.M., Guibourdenche, L., de Villiers, S., Krijgsman, W., 2022b. High-amplitude water-level fluctuations at the end of the Mediterranean Messinian Salinity Crisis: Implications for gypsum formation, connectivity & global climate. Earth Planet. Sci. Lett. 595, 117767.

Antonarakou, A., Kontakiotis, G., Mortyn, P.G., Drinia, H., Sprovieri, M., Besiou, E., Tripsanas, E., 2015. Biotic and geochemical ($\delta^{18}O$, $\delta^{13}C$, Mg/Ca, Ba/Ca) responses of Globigerinoides ruber morphotypes to upper water column variations during the last deglaciation, Gulf of Mexico. Geochim. Cosmochim. Acta 170, 69–93.

Artoni, A.N., Papani, G.I., Rizzini, F.R., Calderoni, M.I., Bernini, M.A., Argnani, A.N., Roveri, M.A., Rossi, M., Rogledi, S., Gennari, R., 2004. The Salsomaggiore structure (Northwestern Apennine foothills, Italy): a Messinian Mountain front shaped by mass-wasting products. GeoActa 3, 107–128.

Artoni, A., Rizzini, F., Roveri, M., Gennari, R., Manzi, V., Papani, G., Bernini, M., 2007. Tectonic & climatic controls on sedimentation in late Miocene Cortemaggiore wedge-top basin (northwestern Apennines, Italy). In: Thrust Belts & Forel& Basins: From Fold Kinematics to Hydrocarbon Systems. Springer, Berlin Heidelberg, pp. 431–456.

Athanasiou, M., Bouloubassi, I., Gogou, A., Klein, V., Dimiza, M.D., Parinos, C., Skampa, E., Triantaphyllou, M.V., 2017. Sea surface temperatures & environmental

conditions during the "warm Pliocene" interval (~ 4.1–3.2 Ma) in the Eastern Mediterranean (Cyprus). Glob. Planet. Chang. 150, 46–57.
Bassetti, M.A., Manzi, V., Lugli, S., Roveri, M., Longinelli, A., Lucchi, F.R., Barbieri, M., 2004. Paleoenvironmental significance of Messinian post-evaporitic lacustrine carbonates in the northern Apennines, Italy. Sediment. Geol. 172 (1-2), 1–18.
Beltran, C., Flores, J.A., Sicre, M.A., Baudin, F., Renard, M., De Rafélis, M., 2011. Long-chain alkenones in the early Pliocene Sicilian sediments (Trubi Formation-Punta di Maiata section): Implications for the alkenone paleothermometry. Palaeogeogr. Palaeoclimatol. Palaeoecol. 308 (3–4), 253–263.
Bemis, B.E., Spero, H.J., Bijma, J., Lea, D.W., 1998. Reevaluation of the oxygen isotopic composition of planktonic foraminifera: Experimental results and revised paleotemperature equations. Paleoceanography 13 (2), 150–160.
Bendle, J.A., Rosell-Melé, A., Cox, N.J., Shennan, I., 2009. Alkenones, alkenoates, & organic matter in coastal environments of NW Scotl&: Assessment of the potential application for sea level reconstruction. Geochem. Geophys. Geosyst. 10 (12), 1–29.
Bertini, A., Martinetto, E., 2011. Reconstruction of vegetation transects for the Messinian–Piacenzian of Italy by means of comparative analysis of pollen, leaf, and carpological records. Palaeogeogr. Palaeoclimatol. Palaeoecol. 304 (3–4), 230–246.
Bigi, G., Castellarin, A., Catalano, R., Coli, M., Cosentino, D., Dal Piaz, G.V., Lentini, F., Parotto, M., Patacca, E., Praturlon, A., Salvini, F., Sartori, R., Scandone, P., Vai, G.B., 1989. Synthetic Structural-Kinematic Map of Italy. C.N.R., Progetto Finalizzato Geodinamica, SELCA Firenze.
Bonaduce, G., Sgarrella, F., 1999. Paleoecological interpretation of the latest Messinian sediments from southern Sicily (Italy). Mem. Soc. Geol. Ital. 54, 83–91.
Bown, P.R. (Ed.), 1998. Calcareous Nannofossil Biostratigraphy. Chapman & Hall, London, pp. 1–31.
Brassell, S.C., Eglinton, G., Marlowe, I.T., Pflaumann, U., Sarnthein, M., 1986. Molecular stratigraphy: a new tool for climatic assessment. Nature 320 (6058), 129–133.
Bulian, F., Kouwenhoven, T.J., Andersen, N., Krijgsman, W., Sierro, F.J., 2022. Reflooding and repopulation of the Mediterranean Sea after the Messinian Salinity Crisis: Benthic foraminifera assemblages and stable isotopes of Spanish basins. Mar. Micropaleontol. 176, 102160.
Camerlenghi, A., 2022. Lingering end to a salinity crisis. Nat. Geosci. 15 (9), 688–690.
Capella, W., Spakman, W., van Hinsbergen, D.J., Chertova, M.V., Krijgsman, W., 2020. Mantle resistance against Gibraltar slab dragging as a key cause of the Messinian Salinity Crisis. Terra Nova 32 (2), 141–150.
Carminati, E., Doglioni, C., 2012. Alps vs. Apennines: the paradigm of a tectonically asymmetric Earth. Earth Sci. Rev. 112 (1–2), 67–96.
Carnevale, G., Landini, W., Sarti, G., 2006. Mare versus Lago-mare: marine fishes and the Mediterranean environment at the end of the Messinian Salinity Crisis. J. Geol. Soc. 163 (1), 75–80.
Carnevale, G., Longinelli, A., Caputo, D., Barbieri, M., Landini, W., 2008. Did the Mediterranean marine reflooding precede the Mio–Pliocene boundary? Paleontological and geochemical evidence from upper Messinian sequences of Tuscany, Italy. Palaeogeogr. Palaeoclimatol. Palaeoecol. 257 (1–2), 81–105.
Carnevale, G., Dela Pierre, F., Natalicchio, M., Walter, L., 2018. Fossil marine fishes and the 'Lago-Mare' event: has the Mediterranean ever transformed into a brackish lake? Newsl. Stratigr. 51 (1), 57–72.
Carnevale, G., Gennari, R., Lozar, F.M.J., Natalicchio, M., Pellegrino, L., Dela Pierre, F., 2019. Living in a deep desiccated Mediterranean Sea: An overview of the Italian fossil record of the Messinian salinity crisis. Boll. Soc. Paleontol. Ital. 58, 109–140.
Caruso, A., Blanc-Valleron, M.M., Da Prato, S., Pierre, C., Rouchy, J.M., 2020. The late Messinian "Lago-Mare" event and the Zanclean reflooding in the Mediterranean Sea: New insights from the Cuevas del Almanzora section (Vera Basin, South-Eastern Spain). Earth Sci. Rev. 200, 102993.
Chu, G., Sun, Q., Li, S., Zheng, M., Jia, X., Lu, C., Liu, T., 2005. Long-chain alkenone distributions and temperature dependence in lacustrine surface sediments from China. Geochim. Cosmochim. Acta 69 (21), 4985–5003.
CIESM, 2008. TheMessinianSalinityCrisismega-depositsto microbiology ± A consensus report. Në. In: Ed., F. (Ed.), pp. 168–pp.
Cita, M.B., 1982. The Messinian salinity crisis in the Mediterranean: a review. Alpine-Mediterranean Geodyn. 7, 113–140.
Clauzon, G., Suc, J.P., Do Couto, D., Jouannic, G., Melinte-Dobrinescu, M.C., Jolivet, L., Estrada, F., 2015. New insights on the Sorbas Basin (SE Spain): the onshore reference of the Messinian Salinity Crisis. Mar. Pet. Geol. 66, 71–100.
Colombero, S., Bonelli, E., Kotsakis, T., Pavia, G., Pavia, M., Carnevale, G., 2013. Late Messinian rodents from Verduno (Piedmont, NW Italy): Biochronological, paleoecological and paleobiogeographic implications. Geobios 46 (1-2), 111–125.
Conte, M.H., Thompson, A., Lesley, D., Harris, R.P., 1998. Genetic & physiological influences on the alkenone/alkenoate versus growth temperature relationship in Emiliania huxleyi & Gephyrocapsa oceanica. Geochim. Cosmochim. Acta 62 (1), 51–68.
Conte, M.H., Weber, J.C., King, L.L., Wakeham, S.G., 2001. The alkenone temperature signal in western North Atlantic surface waters. Geochim. Cosmochim. Acta 65 (23), 4275–4287.
Conte, M.H., Sicre, M.A., Rühlemann, C., Weber, J.C., Schulte, S., Schulz-Bull, D., Blanz, T., 2006. Global temperature calibration of the alkenone unsaturation index (UK′ 37) in surface waters and comparison with surface sediments. Geochem. Geophys. Geosyst. 7 (2).
Corbí, H., Soria, J.M., Lancis, C., Giannetti, A., Tent-Manclús, J.E., Dinarès-Turell, J., 2016. Sedimentological and paleoenvironmental scenario before, during, and after the Messinian Salinity Crisis: the San Miguel de Salinas composite section (western Mediterranean). Mar. Geol. 379, 246–266.
Cosentino, D., Buchwaldt, R., Sampalmieri, G., Iadanza, A., Cipollari, P., Schildgen, T.F., Hinnov, L.A., Ramezani, J., Bowring, S.A., 2013. Refining the Mediterranean "Messinian gap" with high-precision U-Pb zircon geochronology, central and northern Italy. Geology 41 (3), 323–326.
D'Andrea, W.J., Theroux, S., Bradley, R.S., Huang, X., 2016. Does phylogeny control U37K-temperature sensitivity? Implications for lacustrine alkenone paleothermometry. Geochim. Cosmochim. Acta 175, 168–180.
Dela Pierre, F.D., Bernardi, E., Cavagna, S., Clari, P., Gennari, R., Irace, A., Lozar, F., Lugli, S., Manzi, V., Natalicchio, M., Violanti, D., 2011. The record of the Messinian salinity crisis in the Tertiary Piedmont Basin (NW Italy): the Alba section revisited. Palaeogeogr. Palaeoclimatol. Palaeoecol. 310 (3–4), 238–255.
Di Stefano, A., Sturiale, G., 2010. Refinements of calcareous nannofossil biostratigraphy at the Miocene/Pliocene Boundary in the Mediterranean region. Geobios 43 (1), 5–20.
Di Stefano, E., Sprovieri, R., Scarantino, S., 1996. Chronology of biostratigraphic events at the base of the Pliocene. Paleopelagos 6, 401–414.
Esu, D., Girotti, O., 2008. The late Messinian Lago-Mare molluscan assemblage from the Trave Horizon (Colombacci Fm). At Pietralacroce (Ancona, Central Italy). Boll. Soc. Paleontol. Ital. 47 (2), 123–129.
Garcia-Castellanos, D., Estrada, F., Jiménez-Munt, I., Gorini, C., Fernández, M., Vergés, J., De Vicente, R., 2009. Catastrophic flood of the Mediterranean after the Messinian salinity crisis. Nature 462 (7274), 778–781.
Garcia-Castellanos, D., Micallef, A., Estrada, F., Camerlenghi, A., Ercilla, G., Periáñez, R., Abril, J.M., 2020. The Zanclean megaflood of the Mediterranean–Searching for independent evidence. Earth Sci. Rev. 201, 103061.
Gennari, R., Iaccarino, S.M., Di Stefano, A., Sturiale, G., Cipollari, P., Manzi, V., Cosentino, D., 2008. The Messinian–Zanclean boundary in the Northern Apennine. Stratigraphy 5 (3–4), 309–325.
Giunta, S., Morigi, C., Negri, A., Guichard, F., Lericolais, G., 2007. Holocene biostratigraphy and paleoenvironmental changes in the Black Sea based on calcareous nannoplankton. Mar. Micropaleontol. 63 (1–2), 91–110.
Gliozzi, E., Grossi, F., 2008. Late Messinian lago-mare ostracod palaeoecology: a correspondence analysis approach. Palaeogeogr. Palaeoclimatol. Palaeoecol. 264 (3–4), 288–295.
Gould, J., Kienast, M., Dowd, M., 2017. Investigation of the UK37'vs. SST relationship for Atlantic Ocean suspended particulate alkenones: An alternative regression model and discussion of possible sampling bias. Deep-Sea Res. I Oceanogr. Res. Pap. 123, 13–21.
Grossi, F., Gennari, R., 2008. Palaeoenvironmental reconstruction across the Messinian/Zanclean boundary by means of ostracods and foraminifers: the Montepetra borehole (northern Apennine, Italy). Atti Museo Civico Storia Nat. Trieste 53 (Suppl), 67–88.
Grossi, F., Cosentino, D., Gliozzi, E., 2008. Late Messinian Lago-Mare ostracods and palaeoenvironments of the central and eastern Mediterranean Basin. Boll. Soc. Paleontol. Ital. 47 (2), 131–146.
Grothe, A., Sangiorgi, F., Brinkhuis, H., Stoica, M., Krijgsman, W., 2018. Migration of the dinoflagellate Galeacysta etrusca and its implications for the Messinian Salinity Crisis. Newsl. Stratigr. 1.
Gvirtzman, Z., Heida, H., Garcia-Castellanos, D., Bar, O., Zucker, E., Enzel, Y., 2022. Limited Mediterranean Sea-level drop during the Messinian salinity crisis inferred from the buried Nile canyon. Commun. Earth Environ. 3 (1), 216.
Harada, N., Sato, M., Sakamoto, T., 2008. Freshwater impacts recorded in tetra unsaturated alkenones and alkenone sea surface temperatures from the Okhotsk Sea across millennial-scale cycles. Paleoceanography 23 (3).
Henderiks, J., Sturm, D., Šupraha, L., Langer, G., 2022. Evolutionary rates in the Haptophyta: Exploring Molecular and Phenotypic Diversity. J.Marine Sci. Eng. 10 (6), 798.
Herbert, T.D., Lawrence, K.T., Tzanova, A., Peterson, L.C., Caballero-Gill, R., Kelly, C.S., 2016. Late Miocene global cooling and the rise of modern ecosystems. Nat. Geosci. 9 (11), 843–847.
Hsü, K.J., Ryan, W.B., Cita, M.B., 1973. Late Miocene desiccation of the Mediterranean. Nature 242, 240–244.
Huang, Y., Zheng, Y., Heng, P., Giosan, L., Coolen, M.J., 2021. Black Sea paleosalinity evolution since the last deglaciation reconstructed from alkenone-inferred Isochrysidales diversity. Earth Planet. Sci. Lett. 564, 116881.
Iaccarino, S., Papani, G., 1979. In: Istituti di Geologia, Paleontologia, Geografia, Petrografia e Giacimenti Minerari, Mineralogia (Ed.), Il Messiniano dell'Appennino Settentrionale dalla Val d'Arda alla Val Secchia: stratigrafia e rapporti con il substrato e il Pliocene, Volume dedicato a Sergio Venzo. Università degli Studi di Parma, Parma, pp. 15–46.
Iaccarino, S.M., Cita, M.B., Gaboardi, S., Gruppini, G.M., 1999. High-Resolution Biostratigraphy at the Miocene/Pliocene boundary in Holes 974b and 975b, Western Mediterranean. In: Proceedings of the Ocean Drilling Program: Scientific Results, 161, p. 197.
Kaiser, J., Wang, K.J., Rott, D., Li, G., Zheng, Y., Amaral-Zettler, L., Amaral-Zettler, Linda, Arz, Helge W., Huang, Y., 2019. Changes in long chain alkenone distributions and Isochrysidales groups along the Baltic Sea salinity gradient. Org. Geochem. 127, 92–103.
Kontakiotis, G., Besiou, E., Antonarakou, A., Zarkogiannis, S.D., Kostis, A., Mortyn, P.G., Moissette, P., Corn´ee, J.-J., Schulbert, C., Drinia, H., Anastasakis, G., Karakitsios, V., 2019. Decoding Sea surface and paleoclimate conditions in the eastern Mediterranean over the Tortonian-Messinian transition. Palaeogeogr. Palaeoclimatol. Palaeoecol. 534, 109312.
Kontakiotis, G., Butiseacă, G.A., Antonarakou, A., Agiadi, K., Zarkogiannis, S.D., Krsnik, E., Besiou, E., Zachariasse, W.J., Lourens, L., Thivaiou, D., Koskeridou, E., Moisette, P., Mulch, A., Karakitsios, V., Vasiliev, I., 2022. Hypersalinity accompanies tectonic restriction in the eastern Mediterranean prior to the Messinian Salinity Crisis. Palaeogeogr. Palaeoclimatol. Palaeoecol. 592, 110903.

Krijgsman, W., Hilgen, F.J., Raffi, I., Sierro, F.J., Wilson, D.S., 1999. Chronology causes and progression of the Messinian salinity crisis. Nature 400 (6745), 652–655.
Kucera, M., 2019. Determination of past sea surface temperatures. In: Cochran, J.K., Bokuniewicz, H.J., Yager, P.L. (Eds.), Encyclopedia of Ocean Sciences (Third Edition). Academic Press, pp. 490–504.
Laskar, J., Correia, A.C., Gastineau, M., Joutel, F., Levrard, B., Robutel, P., 2004. Long term evolution and chaotic diffusion of the insolation quantities of Mars. Icarus 170 (2), 343–364.
LeGrande, A.N., Schmidt, G.A., 2006. Global gridded data set of the oxygen isotopic composition in seawater. Geophys. Res. Lett. 33 (12).
Lirer, F., Foresi, L.M., Iaccarino, S.M., Salvatorini, G., Turco, E., Cosentino, C., Sierro, F. J., Caruso, A., 2019. Mediterranean Neogene planktonic foraminifer biozonation and biochronology. Earth Sci. Rev. 196, 102869.
Liu, W., Liu, Z., Wang, H., He, Y., Wang, Z., Xu, L., 2011. Salinity control on long-chain alkenone distributions in lake surface waters and sediments of the northern Qinghai-Tibetan Plateau, China. Geochim. Cosmochim. Acta 75 (7), 1693–1703.
Longo, W.M., Theroux, S., Giblin, A.E., Zheng, Y., Dillon, J.T., Huang, Y., 2016. Temperature calibration and phylogenetically distinct distributions for freshwater alkenones: evidence from northern Alaskan lakes. Geochim. Cosmochim. Acta 180, 177–196.
Mancini, A., Nallino, E., Pilade, F., 2023. Toward a Discrimination between Reworked and In Situ Microfossil during the Last Phase of the Messinian Salinity Crisis: Taphonomic Insights from Maccarone Section (Central Italy). Rend. Online Soc. Geol. It, p. 60.
Manzi, V., Roveri, M., Gennari, R., Bertini, A., Biffi, U., Giunta, S., Iaccarino, S.M., Lanci, L., Lugli, S., Negri, A., Riva, A., Rossi, M.E., Taviani, M., 2007. The deep-water counterpart of the Messinian Lower Evaporites in the Apennine foredeep: the Fanantello section (Northern Apennines, Italy). Palaeogeogr. Palaeoclimatol. Palaeoecol. 251, 470–499.
Marlowe, I.T., Green, J.C., Neal, A.C., Brassell, S.C., Eglinton, G., Course, P.A., 1984. Long chain (n-C37–C39) alkenones in the Prymnesiophyceae. Distribution of alkenones & other lipids & their taxonomic significance. Br. Phycol. J. 19 (3), 203–216.
Marzocchi, A., Flecker, R., Van Baak, C.G., Lunt, D.J., Krijgsman, W., 2016. Mediterranean outflow pump: An alternative mechanism for the Lago-mare and the end of the Messinian Salinity Crisis. Geology 44 (7), 523–526.
Merzeraud, G., Achalhi, M., Cornée, J.J., Münch, P., Azdimousa, A., Moussa, A.B., 2019. Sedimentology and sequence stratigraphy of the late-Messinian-early pliocene continental to marine deposits of the Boudinar basin (North Morocco). J. Afr. Earth Sci. 150, 205–223.
Micallef, A., Camerlenghi, A., Garcia-Castellanos, D., Cunarro Otero, D., Gutscher, M.A., Barreca, G., Spatola, L., Facchin, L., Geletti, R., Krastel, S., Gross., F., Urlaub, M., 2018. Evidence of the Zanclean megaflood in the eastern Mediterranean Basin. Sci. Rep. 8 (1), 1078.
Miller, K.G., Mountain, G.S., Wright, J.D., Browning, J.V., 2011. A 180-million-year record of sea level and ice volume variations from continental margin and deep-sea isotopic records. Oceanography 24 (2), 40–53.
Mosca, P., Polino, R., Rogledi, S., Rossi, M., 2010. New data for the kinematic interpretation of the Alps–Apennines junction (Northwestern Italy). Int. J. Earth Sci. 99 (4), 833–849.
Müller, P.J., Kirst, G., Ruhland, G., Von Storch, I., Rosell-Melé, A., 1998. Calibration of the alkenone paleotemperature index U37K′ based on core-tops from the eastern South Atlantic and the global ocean (60 N-60 S). Geochim. Cosmochim. Acta 62 (10), 1757–1772.
Nakamura, H., Sawada, K., Araie, H., Suzuki, I., Shiraiwa, Y., 2014. Long chain alkenes, alkenones and alkenoates produced by the haptophyte alga Chrysotila lamellosa CCMP1307 isolated from a salt marsh. Org. Geochem. 66, 90–97.
Odin, G.S., Lucchi, F.R., Tateo, F., Cosca, M., Hunziker, J.C., 1995. Chapter E7 Integrated stratigraphy of the maccarone section, late messinian (Marche Region, Italy). In: Developments in Palaeontology and Stratigraphy, 15, pp. 531–545.
Orszag-Sperber, F., 2006. Changing perspectives in the concept of “Lago-Mare” in Mediterranean late Miocene evolution. Sediment. Geol. 188, 259–277.
Pellen, R., Popescu, S.M., Suc, J.P., Melinte-Dobrinescu, M.C., Rubino, J.L., Rabineau, M., Marabini, S., Loget, N., Casero, P., Cavazza, W., Head, M.J., 2017. The Apennine foredeep (Italy) during the latest Messinian: Lago-Mare reflects competing brackish and marine conditions based on calcareous nannofossils and dinoflagellate cysts. Geobios 50 (3), 237–257.
Pierre, C., 1999. The oxygen and carbon isotope distribution in the Mediterranean water masses. Mar. Geol. 153 (1–4), 41–55.
Popescu, S.M., Melinte, M.C., Suc, J.P., Clauzon, G., Quillévéré, F., Sütő-Szentai, M., 2008. Marine reflooding of the Mediterranean after the Messinian Salinity Crisis predates the Zanclean GSSP. Reply to the “Comment on ‘Earliest Zanclean age for the Colombacci and uppermost Di Tetto formations of the “latest Messinian” northern Apennines: New palaeoenvironmental data from the Maccarone section (Marche Province, Italy)’by Popescu et al. (2007). Geobios 40 (359–373)” authored by Roveri et al. Geobios 41 (5), 657–660.
Popescu, S.M., Melinte-Dobrinescu, M.C., Suc, J.P., Do Couto, D., 2017. Ceratolithus acutus Gartner and Bukry 1974 (= C. armatus Müller 1974), calcareous nannofossil marker of the marine reflooding that terminated the Messinian salinity crisis: comment on “Paratethyan ostracods in the Spanish Lago-Mare: more evidence for interbasinal exchange at high Mediterranean Sea level” by Stoica et al., 2016. Palaeogeogr. Palaeoclimatol. Palaeoecol. 441, 854–870.
Prahl, F.G., Wakeman, S.G., 1987. Calibration of unsaturation patterns in long-chain alkenones as indicators of paleoceanographic conditions. Nature 330, 367–369.
Prahl, F.G., Muehlhausen, L.A., Zahnle, D.L., 1988. Further evaluation of long chain alkenones as indicators of paleoceanographic conditions. Geochim. Cosmochim. Acta 52 (9), 2303–2310.
Ricci Lucchi, F., 1986. The Oligocene to recent foreland basins of the Northern Apennines. Foreland Basins 103–139.
Rice, A., Nooteboom, P.D., Van Sebille, E., Peterse, F., Ziegler, M., Sluijs, A., 2022. Limited lateral transport bias during export of sea surface temperature proxy carriers in the Mediterranean Sea. Geophys. Res. Lett. 49 (4) e2021GL096859.
Rouchy, J.M., Caruso, A., 2006. The Messinian salinity crisis in the Mediterranean basin: a reassessment of the data and an integrated scenario. Sediment. Geol. 188, 35–67.
Roveri, M., Manzi, V., Bassetti, M.A., Merini, M., Ricci Lucchi, F., 1998. Stratigraphy of the Messinian post-evaporitic stage in eastern Romagna (northern Apennines, Italy). Giorn. Geol. 60 (3), 119–142.
Roveri, M., Bertini, A., Cipollari, P., Cosentino, D., Di Stefano, A., Florindo, F., Gennari, R., Gliozzi, E., Grossi, F., Iaccarino, S., Lugli, S., Manzi, V., Taviani, M., 2008a. “Earliest Zanclean age for the Colombacci and uppermost Di Tetto formations of the «latest Messinian» northern Apennines: New palaeoenvironmental data from the Maccarone section (Marche Province, Italy)” by Popescu et al. (2007) Geobios 40 (359–373). Geobios 41 (5), 669–675.
Roveri, M., Bertini, A., Cosentino, D., Di Stefano, A., Gennari, R., Gliozzi, E., Grossi, F., Iaccarino, S.M., Lugli, S., Manzi, V., Taviani, M., 2008b. A high-resolution stratigraphic framework for the latest Messinian events in the Mediterranean area. Stratigraphy 5 (3-4), 323–342.
Roveri, M., Lugli, S., Manzi, V., Schreiber, B.C., 2008c. The Messinian Sicilian stratigraphy revisited: new insights for the Messinian salinity crisis. Terra Nova 20 (6), 483–488.
Roveri, M., Flecker, R., Krijgsman, W., Lofi, J., Lugli, S., Manzi, V., Sierro, F.J., Bertini, A., Camerlenghi, A., De Lange, G., Govers, R., 2014a. The Messinian Salinity Crisis: past & future of a great challenge for marine sciences. Mar. Geol. 352, 25–58.
Roveri, M., Flecker, R., Krijgsman, W., Lofi, J., Lugli, S., Manzi, V., Sierro, F.J., Bertini, A., Camerlenghi, A., De Lange, G., Govers, R., Hilgen, F.J., Hübscher, C., Meijer, P., Stoica, M., 2014b. The Messinian Salinity Crisis: past and future of a great challenge for marine sciences. Mar. Geol. 352, 25–58.
Roveri, M., Manzi, V., Bergamasco, A., Falcieri, F.M., Gennari, R., Lugli, S., Schreiber, B. C., 2014c. Dense shelf water cascading and Messinian canyons: a new scenario for the Mediterranean salinity crisis. Am. J. Sci. 314 (3), 751–784.
Roveri, M., Lugli, S., Manzi, V., Reghizzi, M., Rossi, F.P., 2020. Stratigraphic relationships between shallow-water carbonates and primary gypsum: insights from the Messinian succession of the Sorbas Basin (Betic Cordillera, Southern Spain). Sediment. Geol. 404, 105678.
Ryan, W.B., 2011. Geodynamic responses to a two-step model of the Messinian salinity crisis. Bull. Soc. Géol. France 182 (2), 73–78.
Schwarzans, W., Carnevale, G., 2022. Bathyal fish otoliths from the Bartonian (eocene) of the turin hill (Piedmont, italy). Rivista Italiana di Paleontologia e Stratigrafia 128 (3).
Schwarzhans, W., Agiadi, K., Carnevale, G., 2020. Late Miocene–Early Pliocene evolution of Mediterranean gobies and their environmental and biogeographic significance. Riv. Ital. Paleontol. Stratigr. 126 (3), 657–724.
Siddall, M., Rohling, E.J., Almogi-Labin, A., Hemleben, C., Meischner, D., Schmelzer, I., Smeed, D.A., 2003. Sea-level fluctuations during the last glacial cycle. Nature 423 (6942), 853–858.
Skejić, S., Arapov, J., Bužančić, M., Ninčević Gladan, Ž., Bakrač, A., Straka, M., Mandić, J., 2021. First evidence of an intensive bloom of the coccolithophore Syracosphaera halldalii in a highly variable estuarine environment (Krka River, Adriatic Sea). Mar. Ecol. 42 (2), e12641.
Spezzaferri, S., Cita, M.B., McKenzie, J.A., 1998. The Miocene/Pliocene boundary in the Eastern Mediterranean: results from Sites 967 and 969. In: Proceedings-Ocean Drilling Program Scientific Results (9-28). National science foundation.
Stoica, M., Krijgsman, W., Fortuin, A., Gliozzi, E., 2018. Reply to "Ceratolithus acutus Gartner and Bukry 1974 (= C. armatus Müller 1974), calcareous nannofossil marker of the marine flooding that terminated the Messinian salinity crisis" by Popescu et al., 2017. Palaeogeogr. Palaeoclimatol. Palaeoecol. 511.
Sun, Q., Chu, G., Liu, G., Li, S., Wang, X., 2007. Calibration of alkenone unsaturation index with growth temperature for a lacustrine species, Chrysotila lamellosa (Haptophyceae). Org. Geochem. 38 (8), 1226–1234.
Taviani, M., Remia, A., Esu, D., Sami, M., 2007. Messinian lago-Mare mollusc fauna from the Gorgona island slope, Tyrrhenian Sea. Geobios 40 (3), 351–358.
Theroux, S., D'Andrea, W.J., Toney, J., Amaral-Zettler, L., Huang, Y., 2010. Phylogenetic diversity and evolutionary relatedness of alkenone-producing haptophyte algae in lakes: implications for continental paleotemperature reconstructions. Earth Planet. Sci. Lett. 300 (3–4), 311–320.
Theroux, S., Toney, J., Amaral-Zettler, L., Huang, Y., 2013. Production and temperature sensitivity of long-chain alkenones in the cultured haptophyte Pseudoisochrysis paradoxa. Org. Geochem. 62, 68–73.
Trend-Staid, M., Prell, W.L., 2002. Sea surface temperature at the last Glacial Maximum: a reconstruction using the modern analog technique. Paleoceanography 17 (4), 17-1.
Trenkwalder, S., Violanti, D., d'Atri, A., Lozar, F., Dela Pierre, F., Irace, A., 2008. The Miocene/Pliocene boundary and the early Pliocene micropaleontological record: new data from the Tertiary Piedmont Basin (Moncucco quarry, Torino Hill, Northwestern Italy). Boll. Soc. Paleontol. Ital. 47 (2), 87–103.
Tzanova, A., Herbert, T.D., Peterson, L., 2015. Cooling Mediterranean Sea surface temperatures during the Late Miocene provide a climate context for evolutionary transitions in Africa and Eurasia. Earth Planet. Sci. Lett. 419, 71–80.
Van Couvering, J.A., Castradori, D., Cita, M.B., Hilgen, F.J., Rio, D., 2000. The base of the Zanclean Stage and of the Pliocene Series. Episodes J. Int. Geosci. 23 (3), 179–187.

Van der Laan, E., Snel, E., De Kaenel, E., Hilgen, F.J., Krijgsman, W., 2006. No major deglaciation across the Miocene-Pliocene boundary: integrated stratigraphy and astronomical tuning of the Loulja sections (Bou Regreg area, NW Morocco). Paleoceanography 21 (3).

Vasiliev, I., Mezger, E.M., Lugli, S., Reichart, G.J., Manzi, V., Roveri, M., 2017. How dry was the Mediterranean during the Messinian salinity crisis? Palaeogeogr. Palaeoclimatol. Palaeoecol. 471, 120-133.e.

Van Dijk, G., Maars, J., Andreetto, F., Hernández-Molina, F.J., Rodríguez-Tovar, F.J., Krijgsman, W., 2023. A terminal Messinian flooding of the Mediterranean evidenced by contouritic deposits on Sicily. Sedimentology 70, 1195–1223.

Vasiliev, I., Karakitsios, V., Bouloubassi, I., Agiadi, K., Kontakiotis, G., Antonarakou, A., Triantaphyllou, M., Gogou, A., Kafousia, N., Zarkogiannis, S., Kaczmar, F., Parinos, C., Pasadakis, N., 2019. Large sea surface temperature, salinity, and productivity-preservation changes preceding the onset of the Messinian Salinity Crisis in the eastern Mediterranean Sea. Paleoceanogr. Paleoclimatol. 34 (2), 182–202.

Violanti, D., Dela Pierre, F., Trenkwalder, S., Lozar, F., Clari, P., Irace, A., D'Atri, A., 2011. Biostratigraphic and palaeoenvironmental analyses of the Messinian/Zanclean boundary and Zanclean succession in the Moncucco quarry (Piedmont, northwestern Italy). Bull. Soc. Géol. France 182 (2), 149–162.

Wang, Z., Liu, Z., Zhang, F., Fu, M., An, Z., 2015. A new approach for reconstructing Holocene temperatures from a multi-species long chain alkenone record from Lake Qinghai on the northeastern Tibetan Plateau. Org. Geochem. 88, 50–58.

Wang, K.J., Huang, Y., Majaneva, M., Belt, S.T., Liao, S., Novak, J., Cabedo-Sanz, P., 2021. Group 2i Isochrysidales produce characteristic alkenones reflecting sea ice distribution. Nat. Commun. 12 (1), 15.

Williams, M., Haywood, A.M., Taylor, S.P., Valdes, P.J., Sellwood, B.W., Hillenbrand, C. D., 2005. Evaluating the efficacy of planktonic foraminifer calcite delta O-18 data for sea surface temperature reconstruction for the late Miocene. Geobios 38, 843–863.

Zheng, Y., Heng, P., Conte, M.H., Vachula, R.S., Huang, Y., 2019. Systematic chemotaxonomic profiling and novel paleotemperature indices based on alkenones and alkenoates: potential for disentangling mixed species input. Org. Geochem. 128, 26–41.

Zink, K.G., Leythaeuser, D., Melkonian, M., Schwark, L., 2001. Temperature dependency of long-chain alkenone distributions in recent to fossil limnic sediments and in lake waters. Geochim. Cosmochim. Acta 65 (2), 253–265.